Journal Pre-proof

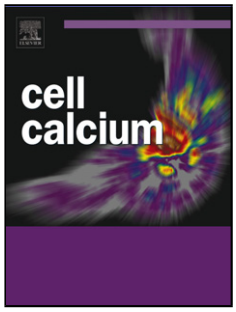

The *Schistosoma mansoni* tegumental allergen protein, SmTAL1: binding to an IQ-motif from a voltage-gated ion channel and effects of praziquantel

Charlotte M. Thomas, David J. Timson

PII: S0143-4160(20)30003-8

DOI: https://doi.org/10.1016/j.ceca.2020.102161

Reference: YCECA 102161

To appear in: *Cell Calcium*

Received Date: 6 December 2019

Revised Date: 30 December 2019

Accepted Date: 10 January 2020

Please cite this article as: Thomas CM, Timson DJ, The *Schistosoma mansoni* tegumental allergen protein, SmTAL1: binding to an IQ-motif from a voltage-gated ion channel and effects of praziquantel, *Cell Calcium* (2020), doi: https://doi.org/10.1016/j.ceca.2020.102161

The *Schistosoma mansoni* tegumental allergen protein, SmTAL1: binding to an IQ-motif from a voltage-gated ion channel and effects of praziquantel

Charlotte M. Thomas[1,2] and David J Timson[3]*

[1] School of Biological Sciences and Institute for Global Food Security, Queen's University Belfast, Medical Biology Centre, 97 Lisburn Road, Belfast, BT9 7BL, UK.

[2] Current address: Division of Infection and Immunity, The Roslin Institute, University of Edinburgh, Easter Bush Campus, Midlothian, EH25 9RG, UK.

[3] School of Pharmacy and Biomolecular Sciences, University of Brighton, Huxley Building, Lewes Road, Brighton, BN2 4GJ, UK.

*Author to whom correspondence should be addressed at School of Pharmacy and Biomolecular Sciences, University of Brighton, Huxley Building, Lewes Road, Brighton, BN2 4GJ. UK.

Telephone +44(0)1273 641623

Fax +44(0)1273 642090

Email d.timson@brighton.ac.uk

Graphical abstract

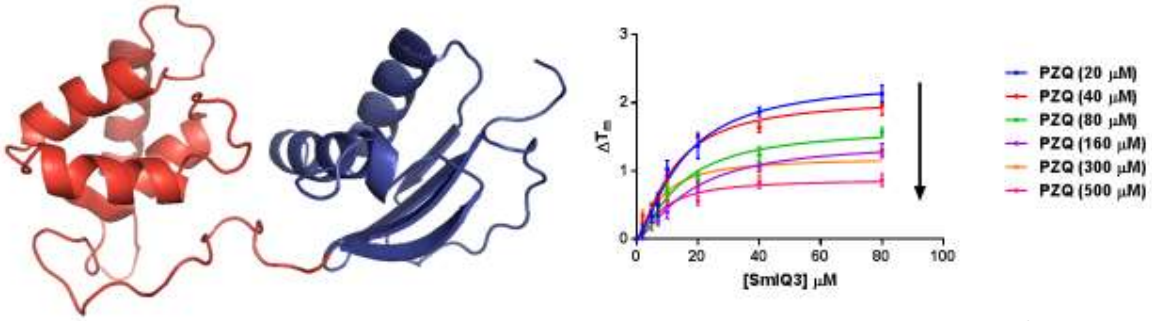

Highlights

- SmTAL1 binds four calcium ions per dimer
- There are cooperative interactions between binding sites
- SmTAL1 binds praziquantel non-cooperatively
- SmTAL1 interacts with an IQ-motif from $SmCa_v1B$
- Praziquantel interferes with this interaction in a complex manner

Abstract

SmTAL1 is a calcium binding protein from the parasitic worm, *Schistosoma mansoni.* Structurally it is comprised of two domains – an N-terminal EF-hand domain and a C-terminal dynein light chain (DLC)-like domain. The protein has previously been shown to interact with the anti-schistosomal drug, praziquantel (PZQ). Here, we demonstrated that both EF-hands in the N-terminal domain are functional calcium ion binding sites. The second EF-hand appears to be more important in dictating affinity and mediating the conformational changes which occur on calcium ion binding. There is positive cooperativity between the four calcium ion binding sites in the dimeric form of SmTAL1. Both the EF-hand domain and the DLC-domain dimerise independently suggesting that both play a role in forming the SmTAL1 dimer. SmTAL1 binds non-cooperatively to PZQ and cooperatively to an IQ-motif

from $SmCa_V1B$, a voltage-gated calcium channel. PZQ tends to strengthen this interaction, although the relationship is complex. These data suggest the hypothesis that SmTAL1 regulates at least one voltage-gated calcium channel and PZQ interferes with this process. This may be important in the molecular mechanism of this drug. It also suggests that compounds which bind SmTAL1, such as six from the Medicines for Malaria Box identified in this work, may represent possible leads for the discovery of novel antagonists.

Keywords: calcium binding protein; EF-hand; praziquantel; IQ-motif; schistosomiasis; voltage-gated calcium channel

1. Introduction

In trematodes and some other helminths, there is a family of unusual calcium binding proteins. These proteins are characterised by having an N-terminal domain with two EF-hand motifs and a C-terminal dynein light chain (DLC) like domain [1, 2]. Thus, the proteins have an N-terminal domain which resembles the globular heads of calmodulin. This is joined by a flexible linker to a C-terminal domain which has very high structural similarity to members of the DLC family (Figure 1) [3-5]. Proteins from this family have been identified and characterised in a number of species including *Schistosoma mansoni*, *Schistosoma japonicum*, *Schistosoma haematobium*, *Fasciola hepatica*, *Fasciola gigantica*, *Opisthorchis viverrini* and *Clonorchis sinensis* [6-20]. In general, these proteins bind to calcium ions, although there are some exceptions, for example *S. mansoni* tegumental allergen-like (TAL) protein 3 (SmTAL3 or Sm20.8) [10, 16]. The 13 *S. mansoni* TAL proteins are probably the best characterised group of proteins from this family. Several of these TAL proteins have been implicated in eliciting IgE-mediated immune responses in the host [11, 21]. The proteins have different tissue and life cycle stage expression profiles and it is clear from the available data that they also vary in terms of their ion

and drug binding properties [10, 11, 16]. There is limited data on the *in vivo* roles of these proteins. One early report demonstrated that SmTAL3 and a dynein light chain form part of a larger complex suggesting that one function may be to regulate microtubule motors [22].

We have previously demonstrated that, despite similarities in sequence and predicted structure, that members of this protein family have different biochemical properties. For example, of the four characterised family members from *F. hepatica*, one dimerises in response to the presence of calcium ions (FhCaBP4), one is converted from a dimer to a monomer by calcium ions (FhCaBP3) and the oligomeric states of the two are unaffected by this ion (FhCaBP1 and FhCaBP2) [12-15]. In the case of the 13 family members from *S. mansoni*, two do not appear to bind calcium ions at all (SmTAL3 and SmTAL5) [10, 16]. FhCaBP2 binds calcium (and other divalent ions) primarily through its second EF-hand motif [13]. However, there is evidence from sequence analysis of the EF-hands to suggest that the some family members from *S. mansoni* (SmTAL7, SmTAL9, SmTAL10 and SmTAL13) bind calcium at primarily at either the first EF-hand motif [16].

SmTAL1 has an increased resistance to thermal denaturation and increased resistance to proteolytic digestion in the presence of praziquantel (PZQ), providing evidence for an interaction with this drug which stabilises the structure of the protein [10]. SmTAL4, SmTAL5 and SmTAL8 are all destablised by PZQ suggesting that the drug may bind to partially unfolded forms of these proteins, promoting lower overall stability [16]. These interactions with SmTAL proteins are particularly interesting since PZQ is the drug of choice for treating *S. mansoni* infections. The drug is cheap, effective and has few significant side effects [23]. However, its mechanism of action is unknown although it is generally accepted that it disrupts calcium homeostasis, potentially through the antagonism of voltage-gated calcium channels [23-26]. The existence of an *in vitro* interaction between the drug and SmTAL1 (and other family members) does not, of course, prove that these proteins are pharmacologically relevant targets of PZQ. Nevertheless their documented biochemical activity as calcium binding proteins makes it tempting to suggest that they may be implicated in the molecular mechanism of action of

this drug. Although few, if any, cases of *bone fide* resistance to PZQ have been reported, it seems likely that resistance will eventually emerge, just as it has to most major classes of antibacterial drug [27-30]. Here we present a detailed, biochemical study of SmTAL1 focusing on its ion and drug binding activities, and probing its ability to interact with IQ-motifs from voltage-gated calcium channels.

2. Materials and Methods

2.1 Expression and purification of wild-type SmTAL1, SmTAL1 variants and SmTAL1 domains

Wild-type SmTAL1 was expressed in, and purified from, *Escherichia coli* Rosetta(DE3) as a hexa-histidine fusion protein. DNA encoding the coding sequence was amplified by PCR from a plasmid used for GST-fusion protein expression of SmTAL1 which was kindly supplied by Dr Colin Fitzsimmons (University of Cambridge, UK) [10, 11]. The amplicon was inserted into the vector pET-46 Ek/LIC according to the manufacturer's instructions (Merck, Nottingham, UK). This plasmid was transformed into Rosetta(DE3) cells and single recombinant colonies were picked and cultured overnight, shaking at 30 °C, in 5 ml of LB (Miller) broth (Foremedium, UK), supplemented with 100 µg ml^{-1} ampicillin and 34 µg ml^{-1} chloramphenicol. These starter cultures were used to inoculate larger cultures (1 L LB broth, supplemented with 100 µg ml^{-1} ampicillin and 34 µg ml^{-1} chloramphenicol), which were grown at 30 °C for a further 8-9 h before induction with 0.3 g IPTG (1.3 mM final concentration). Cells were harvested by centrifugation (4200 g for 20 min), resuspended in approximately 20 ml of buffer R (50 mM Hepes-OH, pH 7.5, 150 mM NaCl, 10%(v/v) glycerol) and frozen at -80 °C. The protein was purified using cobalt affinity resin (His-select, Sigma, Poole, UK) as previously described for other members of the SmTAL family [16].

The expression plasmid was mutated using the QuikChange protocol [31] in order to generate expression vectors for the SmTAL1 variants E32A and D59A. All mutations were verified by DNA sequencing (GATC, London, UK). These variants were expressed and purified using the same protocol

as the wild-type. DNA sequences encoding the N-terminal, EF-hand domain domain (residues 1-99) and the C-terminal, DLC-like domain (residues 100-190) were amplified by PCR and inserted into the vector pET46 Ek/LIC (Figure 1). Following verification of the DNA sequences, the corresponding proteins were expressed and purified using the same protocol as the wild-type.

2.2 Native gel electrophoresis

Proteins were resolved by 6 % discontinuous native-PAGE at pH 8.8 [32, 33]. The full-length protein was electrophoresed for approximately 2 h, whereas EF-hand and DLC-like domain protein fragments were electrophoresed for 80 min. Variant proteins were electrophoresed for the same length of time as the corresponding wild-type protein.

2.3 Protein-protein crosslinking

For dimerisation assays, SmTAL1 proteins (10 – 60 µM), or the monomeric control protein, human galactokinase (HsGALK1, prepared as previously described [34, 35]; 15 µM), were incubated at *37* ^{o}C for 45 min in buffer R, supplemented with either EGTA, or EGTA and a two-molar excess of calcium chloride. Where required PZQ (100-500 µM), or DMSO (1 % v/v) was also included in the reaction mixture. After this time, *bis*(sulfosuccinimidyl) suberate (BS^3; 50-500 µM [36]) was added to each protein sample, to a final volume of 10 µl. Samples were incubated for a further 1 h at 37 ^{o}C, and the reaction terminated by the addition of 10 µl SDS-PAGE loading buffer (120 mM Tris-HCl, pH 6.8, 20% (v/v) glycerol, 0.005% (w/v) bromophenol blue, 1% (w/v) DTT, 4% (w/v) SDS). Samples were then heated to 95 °C for 5 min, resolved on 15 % SDS-PAGE, and visualised by staining with Coomassie blue.

2.4 Densitometry

Densitometry analysis was performed using MyImageAnalysis software, version 2.0 (Thermo Scientific, UK). Gel images were checked to ensure that no saturated pixels were present; those gels with pixel saturation and/ or uneven staining were omitted from analyses. As protein bands were not of equal sizes, the area of each band was selected by eye, and density estimated by dividing the intensity of the band by the number of pixels within each selected area. Densities were background-corrected by selecting six random areas distant from protein bands, and subtracting the mean density from each data point. In crosslinking assays, the change in density was determined by subtracting the background-corrected density of the lower molecular weight band (representing of the SmTAL1 monomer) at a given concentration of SmIQ3, from the corresponding band in the absence of peptide. The change in density was expressed as a percentage, and plotted against the concentration of SmIQ3 peptide at each step of the titration. The relative half-maximal effect (EC_{50}) was estimated by non-linear regression, as implemented in GraphPad Prism, v6.0 (GraphPad Software Inc, CA, USA), using the hyperbolic binding equation: $Y = Y_{max}$ [SmIQ3]/ EC_{50} + [SmIQ3] (Equation 1); where Y denotes the change in density (%), at a given concentration of peptide ([SmIQ3]), and Y_{max} represents the maximum value of Y.

2.5 Limited proteolysis

SmTAL1, and protein fragments corresponding to the SmTAL1 EF-hand and DLC-like domains (7-20 µM) were analysed by limited proteolysis with chymotrypsin. Protein samples were incubated at 37 ^{o}C for 1 h in the presence of calcium chloride (800 µM), in buffer R supplemented with the appropriate drug (250 µM), or DMSO (final concentration, 1 % v/v). After this time, chymotrypsin (600-800 nM) was added, and the reaction incubated for a further 1 h at 37 ^{o}C, and then terminated by the addition of an equal volume of SDS-PAGE loading buffer. Similar assays were conducted with the control protein, recombinant human UDP-galactose 4'-epimerase (HsGALE, prepared as previously described [37]; 40 µM). Protein samples were then heated to 95 °C for 5 min, and resolved on 15 % SDS-PAGE. The resulting digestion patterns were visualised using Coomassie blue stain.

2.6 Medicines for Malaria Venture (MMV) "malaria box" compounds

The Medicines for Malaria Venture (MMV) (Geneva, Switzerland; Durham, USA), provided 400 compounds with activity against malarial parasites, known as the "Malaria Box" [38]. A subset of these compounds, constituting "plate A" (batch number: April 2013), were used in this thesis (plate map available at: https://www.mmv.org/research-development/open-source-research/open-access-malaria-box). Compounds were provided in a 96-well plate format, dissolved in 100 % DMSO, at a stock concentration of 10 mM [39], and stored at -80 ^{o}C until use. Working dilutions (1/10) were made in 10 mM Hepes (pH 7.4). Assays were performed at a final concentration of 100 µM, ensuring that that the drug-delivery vehicle, DMSO, did not exceed a final concentration of 1 % (v/v).

2.7 Peptides

Peptides corresponding to IQ-motifs were identified from the sequences of the *S. mansoni* voltage-gated calcium channels, SmCa$_v$1A, SmCa$_v$1B and SmCa$_v$2A) as previously described [33]. Synthetic peptides (23-mers in accordance with previous work [33, 40-42]) were manufactured commercially (EZBiolab, IN, USA) with each sequence was N-terminal acetylated and C-terminal amidated. Molecular masses were verified by mass spectrometry by the manufacturer, and each peptide stock had an estimated purity of >95 %. Lyophilised peptides were reconstituted in sterile, deionized water to a concentration of 1 mM, and stored at -80 °C. Once defrosted, peptide stocks were either used immediately, or discarded.

2.8 Fluorescence methods

Fluorescence measurements were made in 96-well black plates using a Spectra Max Gemini XS fluorescence plate-reader, using SOFTmax PRO software. Stock solutions of the hydrophobic probe,

anilinonaphthalene-8-sulfonate (ANS) (Sigma Aldrich, UK), were prepared in sterile, deionized water, and shielded from light; working dilutions were prepared in Hepes buffer, pH 7,5. Excitation was set to 350 nm, and emission spectra were collected from 410 to 510 nm. Reactions were performed in triplicate and spectra were background-corrected using control samples with the appropriate buffer solution. For ion-binding assays, proteins (15 µM), were incubated for 30 min at 37 ^{o}C in Hepes buffer, supplemented with either EGTA (1 mM), or EGTA (1 mM) and the appropriate ion solution (2 mM). ANS (36 µM) was then added to each well, to a final volume of 100 µl. Samples were mixed, covered with a plate (to eliminate direct light), and incubated for a further 60 min at 37 ^{o}C before spectra were collected.

For drug binding assays with ANS, proteins (10 µM), were incubated for 30 min at 37 ^{o}C in Hepes buffer pH 7.5, supplemented with either EGTA (1 mM), or EGTA (1 mM) and calcium chloride (2 mM). After which time, DMSO (1 % v/v), or the appropriate drug (100 µM) was added. Reactions were mixed and incubated for a further 45 min at 37 ^{o}C, before the addition of ANS (36 µM). The reactions were incubated for a further 60 min at 37 ^{o}C, before analysis.

For intrinsic fluorescence measurement, excitation was set to 280 nm, and emission spectra were collected from 330 to 400 nm. All samples were prepared in Hepes buffer pH 7.5 supplemented with dithiothreitol (DTT; 1 mM). Reactions were performed in triplicate, in 96-well black plates, and spectra were background-corrected using control samples with the appropriate buffer solution. Proteins (10 µM), were incubated in the presence of calcium chloride (1 mM) for 30 min at 37 ºC, prior to the addition of DMSO (1 % v/v), or the appropriate drug (100 µM). Samples were then mixed and allowed to incubate at 37 °C for a further 1.5 h, before analysis.

2.9 Analytical methods

Differential scanning fluorimetry (DSF) was performed as previously described [16]. Protein concentrations were estimated using the method of Bradford with BSA as a standard [43]. Free calcium ion concentrations ($[Ca^{2+}]_{free}$) were estimated using MaxChelator calculator, v1.3 (https://web.stanford.edu/~cpatton/CaEGTA-TS.htm) [44, 45].

3. Results and Discussion

3.1 Both EF-hands in SmTAL1 interact with calcium ions

In SmTAL1, both EF-hands adhere to the consensus sequence, apart from the inclusion of a glutamine residue at the central loop position of the first EF-hand, which (according to homology modelling), is not predicted to affect the overall fold of the motif (Supplementary Figure S1) [10]. However, these predictions are not consistent with experimental data collected on FhCaBP2, in which an alanine substitution, introduced at the *Z* coordinating position of the second EF-hand largely abolished calcium binding by this protein thus implying that the second EF-hand represented the main calcium binding site [13]. Given that the EF-sites of SmTAL1 and FhCaBP2 share considerable sequence similarity (in the coordinating ligand positions), it was hypothesised that both proteins bind calcium primarily through the second EF-hand. To test this hypothesis, full-length SmTAL1 and a fragment corresponding to the EF-hand domain were used in site-directed mutagenesis experiments.

To investigate whether the first EF-hand played a role in calcium binding, a glutamic acid to alanine variation was introduced at residue 32 (E32A), corresponding to the *-Z* coordinating position. Given the critical role of this bidentate ligand in the formation of the ion coordination sphere [46], the resulting full-length and EF-hand domain variants (designated SmTAL1-E32A and EF-E32A, respectively), would not be expected to coordinate calcium ions at the first EF-hand. Although the introduction of an equivalent variation in the second EF-hand would seem to be the obvious choice for probing calcium binding at this site, it was reasoned that this may not be a viable option. Given

that the bulk of the Ca^{2+}-dependent conformational change is mediated by the second EF-hand sequence in calmodulin [47], the introduction of a variation at the *-Z* coordinating position of this motif could affect the overall stability of the EF-hand domain, potentially altering the conformation of the first EF-hand and confounding interpretation of the binding data [48]. Moreover, the positioning of this residue at the exiting helix (which helps to define the external boundaries of the EF-hand domain), would be expected to exacerbate these effects [49]. Therefore, since the introduction of an asparagine to alanine variation at the *Z* coordinating position of the second EF-hand had abolished ion-binding activity in FhCaBP2 [13], it was reasoned that an equivalent variation (D59A) in the SmTAL1 EF-hand domain, would be better suited for probing ion binding at the second EF-hand, without disturbing the overall structure of the EF-hand domain. These proteins were designated SmTAL1-D59A and EF-D59A, for the variations in the full-length protein and EF-hand domains respectively (Figure 1).

Full-length SmTAL1, a protein fragment corresponding to the EF-hand domain, four variant proteins (SmTAL1-E32A, EF-E32A, SmTAL1-D59A and EF-D59A) and a fragment corresponding to the DLC-like domain of the protein (which does not contain the EF-hand motifs required for calcium chelation), were expressed in, and purified from, *E. coli* (Supplementary Figure S2). These proteins were resolved under discontinuous native-PAGE and, in accordance with previous studies, the calcium-specific chelator EGTA was used to remove any endogenously bound calcium ions [10, 12-16]. Native-PAGE assays revealed that the electrophoretic mobility of full-length SmTAL1 was increased in the presence of EGTA (compared to untreated protein sample), whereas the addition of a molar excess of calcium ions to the EGTA-treated protein reduced the electrophoretic mobility (Figure 2). Thus, SmTAL1 was capable of reversibly binding calcium ions under the conditions of the assay, and was likely to be partially calcium-bound in the untreated protein sample. These data are consistent with previous native-PAGE and DSF assays, which implied that SmTAL1 had pre-associated with calcium ions during the expression/ purification process [10].

In addition to calcium ions, the full-length protein was shown to interact with manganese ions, displaying an intermediate shift, previously observed in native-PAGE assays with the *S. mansoni* calmodulin, SmCaM1 (Figure 2) [33]. A similar native PAGE profile was observed in assays with the EF-hand domain fragment, but not in assays with the DLC-like domain, thereby confirming that (as expected) the EF-hand domain is responsible for divalent cation binding (Figure 2). Binding of SmTAL1 to magnesium and cadmium ions was not detected in this experiment (Figure 2).

The ion binding profiles of SmTAL1-E32A and EF-E32A generally reflected those of the corresponding wild-type proteins (Figure 2). The electrophoretic mobility of both E32A variants was increased in the presence of EGTA (compared to untreated protein sample), whereas the addition of calcium ions to EGTA-treated protein reduced the electrophoretic mobility (Figure 2). Conversely, apart from a smear on the gel with SmTAL1-D59A in the presence of cadmium ions (which was likely to represent partial unfolding), binding was not detected with the D59A variant, thus implying that calcium chelation and subsequent conformational changes are likely to be mediated by the second EF-hand (Figure 2).

However, it should be stressed that the absence of a mobility shift under non-denaturing native-PAGE does not prove absence of ion binding. These assays do not detect transient ion binding, nor do they report on binding events which are not accompanied by a measurable conformational change. Several other members of the SmTAL protein family also failed to display a mobility shift under non-denaturing native-PAGE, but were subsequently shown to bind divalent ions in DSF assays [16]. Moreover, analysis of the migration pattern of the wild-type and E32A variant of the EF-hand domain, indicated that the first EF-hand may play an indirect role in calcium binding. The magnitude of the mobility shift accompanying calcium chelation was considerably larger in the wild-type EF-hand fragment *versus* EF-E32A (Figure 2; box). This suggests that, while SmTAL1-E32A is able to bind calcium ions, the conformational changes it undergoes are different to those in the wild-type protein.

To further explore these phenomena, full-length SmTAL1, the EF-hand domain, and two EF-hand variants (EF-E32A and EF-D59A), were analysed in the presence of the hydrophobic probe,

anilinonaphthalene-8-sulfonate (ANS), which is a sensitive indicator of conformational changes in EF-hand proteins which result in increased surface hydrophobicity of the protein [50]. ANS displayed the expected fluorescence emission spectrum when incubated in the presence of SmTAL1, and excited at 350 nm; a broad peak was observed, with λ_{max} at approximately 460 nm in the presence of EGTA, or 465 nm in the presence of a two-fold molar excess of calcium chloride (Figure 3; Supplementary Table S1). This red shift in emission spectra was accompanied by a substantial increase in fluorescence intensity providing further evidence of Ca^{2+}-dependent conformational change in SmTAL1. Similar effects were observed with the SmTAL1 EF-hand domain, but not with a fragment corresponding to the DLC-like domain, which exhibited no significant changes in fluorescence intensity, and a constant λ_{max} at 460 nm (Figure 3; Supplementary Table S1).

Wild-type SmTAL1 and the EF-hand fragment underwent a similar increase in ANS fluorescence upon the addition of manganese ions, and, in both instances, this was also accompanied by a red shift in emission spectra (Figure 3; Supplementary Table S1). Thus, it seems likely that calcium and manganese ions elicit a similar conformational response at the EF-hand domain. When either EF-hand variant (EF-E32A or EF-D59A) was incubated with ANS in the presence of calcium ions, a small, but statistically significant increase in fluorescence intensity was detected *versus* the EGTA-treatment group (Supplementary Table S1). Since an effect in the presence of calcium was detected in both variants, this suggested the possibility of two calcium binding sites in the EF-hand domain. Despite a significant increase in ANS fluorescence intensity upon calcium binding, this change in fluorescence intensity was not accompanied by a red shift in emission spectra in assays with EF-E32A or EF-D59A. When the wild-type EF-hand fragment was incubated with ANS, it was noted that emission spectra were red-shifted in the untreated protein sample *versus* the EGTA- treatment group, and the fluorescence intensity at λ_{max} significantly increased (Supplementary Table S1). Given that a similar ANS profile was recorded in the presence of excess calcium, this suggested that a sizeable proportion of untreated protein species had pre-associated with calcium ions during the expression/ purification process. Conversely, when the untreated EF-E32A variant was incubated with ANS, there was no significant difference between

untreated and EGTA-treated samples, and no shift in emission spectra; the same was true of the EF-D59A variant (Supplementary Table S1), implying less pre-association with calcium ions. Thus, the EF-hand variants (EF-E32A and EF-D59A) either have a lower affinity for calcium ions (*versus* the wild-type EF-hand fragment), or exhibit a less conformational change upon binding this ion.

SmTAL1 was previously shown to undergo an increase in thermal stability upon calcium binding, as measured by the "melting point" (T_m) of the protein upon thermal denaturation [10]. Thus, DSF was used to probe for calcium binding in wild-type SmTAL1 and two full-length variants, SmTAL1-E32A and SmTAL1-D59A (Figure 4). Note that it was not possible to get reliable thermal stability measurements for the SmTAL1 EF-hand domain (or the two EF-hand variants). As expected, wild-type SmTAL1 underwent a dose-dependent increase in thermal stability when titrated with calcium ions, consistent with binding to the native, folded form of the protein, under the temperatures and conditions of the assay [51, 52] (Figure 4). These effects were also observed with SmTAL1-E32A and SmTAL1-D59A (Figure 4), providing further evidence that SmTAL1 contains two functional calcium binding sites.

Taken together, these data imply distinct roles for the two EF-hand motifs. Since EF-E32A undergoes a Ca^{2+}-dependent mobility shift in native-PAGE assays, whereas EF-D59A does not (Figure 2), it seems likely that the interaction with the second EF-hand motif is longer lasting and contributes more to the Ca^{2+}-dependent conformational change. The first EF-hand is likely to have a more transient interaction with calcium ions. Both EF-hands appear able to function (partly) independently of each other: disruption of one site does not completely abolish binding at the other site. However, the two sites also influence each other. Disruption of the first site alters the effects of binding at the second site as evidenced by native-PAGE.

3.2 There is cooperativity between the two EF-hands in SmTAL1

To permit a more accurate assessment of the binding data, titrations were corrected to determine the concentration of free calcium ions ($[Ca^{2+}]_{free}$), using the MaxChelator. Semi log plots of the data displayed a characteristic sigmoidal shape, with clearly-defined top (Y_{max}) and bottom (Y_{min}) plateaus (Figure 4). However, it was noted that the gradient of the linear phase differed substantially between each dataset, with a notably steeper gradient for the wild-type protein compared to either variant. Thus, binding isotherms were optimised against a three-parameter logistic regression (3PL) model (which assumes a non-cooperative binding mechanism), and a four-parameter (4PL) model (which makes no assumptions on cooperativity).

Binding data for wild-type SmTAL1 and SmTAL1-D59A were best described by the 4PL model, yielding a Hill slope of 3.99 for the wild-type protein, or 1.75 for the SmTAL1-D59A variant (Table 1). Given that Hill slopes > 1.0, indicate positive cooperativity [53], this suggests that both proteins contained multiple, cooperative calcium binding sites. Accordingly, the corresponding Scatchard plots exhibited a "concave-down" curve (Figure 4), which is also characteristic of positive cooperativity [53]. Conversely, as binding data for SmTAL1-E32A were best described by the 3PL model (which has a fixed Hill slope of 1.0) (Table 1), this indicated the occurrence of a single, non-cooperative calcium binding site at the EF-hand domain. Indeed, it should be noted that curve fitting to the 4PL model also generated a Hill slope of approximately 1.0 (data not shown); thus, calcium binding by SmTAL1-E32A is unlikely to be cooperative. Interestingly, the Scatchard plot for SmTAL1-E32A adopted a non-linear, concave-down curve with an intercept on the y-axis (Figure 4). Although non-cooperative binding schemes generally result in a linear Scatchard plot, the occurrence of a non-linear plot that intersects the y-axis can indicate instability [53]. Thus, it is possible that the E32A mutation destabilises the EF-hand domain at low ligand concentrations (consistent with the blurring effect observed in native-PAGE assays with this protein).

The occurrence of up to four cooperative calcium binding sites in the wild-type protein could be explained by positive cooperativity between the four calcium ion binding sites in a dimer. (Note that

the Hill coefficient is not, necessarily equal to the number of binding sites, but does set an upper limit for that number [54].) If it is assumed that calcium binding occurs solely at the first EF-hand for SmTAL1-D59A, and solely at the second EF-hand for SmTAL1-E32A, then the then the occurrence of (at least) two cooperative calcium binding sites in the SmTAL1-D59A variant, may suggest one of two scenarios: either the D59A mutation does not fully deactivate calcium binding at the second EF-hand, or SmTAL1-D59A also exists as a cooperative dimer. If the second scenario applies, then the observation that E32A abolishes positive cooperativity, implies that the first EF-hand plays an important role in cooperative binding. Given that the apparent dissociation constant ($K_{d,\ app}$) for calcium binding was not significantly altered between wild-type SmTAL1 and the SmTAL1-E32A variant (with an estimated $K_{d,\ app}$ of approximately 0.23 µM for both proteins) (Table 1), yet was significantly increased ($K_{d,\ app} \approx 0.38$ µM) in the context of the D59A variant, it may be concluded that the overall calcium affinity of the SmTAL1 EF-hand domain is largely dictated by the second EF-hand.

3.3 Both the EF-hand domain and the DLC-like domain of SmTAL1 dimerise

SmTAL1 has previously been shown to dimerise and this dimerization is not affected by the presence or absence of calcium ions [10]. To explore the oligomeric state of SmTAL1 the fragments corresponding to the EF-hand and DLC-like domains of the protein, as well as two EF-hand variants (EF-E32A and EF-D59A), were analysed for their ability to crosslink in the presence of the chemical crosslinker, BS^3. These assays indicated that each SmTAL1 protein fragment formed a higher molecular mass band on SDS-PAGE gels when incubated in the presence of the crosslinker (Figure 5). Since this band represented a protein species of approximately twice the predicted molecular mass of the monomer (~ 25 kDa), this suggested that both (EF-hand and DLC-like) domains contribute to the formation of SmTAL1 homodimers. Furthermore, in each instance, the extent of dimerisation was unaffected by the presence of calcium, manganese or magnesium ions (Figure 5).

Interestingly, since the wild-type EF-hand protein was crosslinked under similar conditions to EF-variants, EF-E32A and EF-D59A (Figure 5), this suggested that dimerisation was unaffected by these changes. Thus, while a functional first EF-hand is important for calcium binding and the overall conformational homogeneity of the full-length protein (as evidenced by native-PAGE assays with SmTAL1-E32A; Figure 2), there is no experimental evidence to suggest that calcium binding at this site is required for dimerisation of the SmTAL1 EF-hand domain.

3.4 Calmodulin antagonists and other drugs bind primarily to the EF-hand domain of SmTAL1

Structural studies on calmodulin (CaM) have demonstrated that antagonists of this protein, such as CPZ, W7 and TFP, bind within deep hydrophobic pockets, formed by conformational changes in the N- and C-terminal EF-hand domains upon calcium binding [55, 56]. This stabilises a compact conformation which essentially antagonises interactions with other target molecules [56, 57]. Thiamylal (ThA), an anaesthetic compound, which has previously been shown to antagonise interactions between CaM and calcineurin has an unmapped binding site [58]. However, in FhCaBP2, interaction with this drug is also mediated by the EF-hand domain [13]. The antischistosomal drug, PZQ, has been shown to bind an *S. mansoni* myosin light chain (MLC), an EF-hand protein which has structural similarity to CaM [59]. Given these lines of evidence, it is reasonable to postulate that drug interactions with SmTAL1 are likely to occur predominantly *via* the EF-hand domain. Therefore, to map putative drug interactions with SmTAL1, limited proteolysis was used with the full-length protein, and protein fragments corresponding to the individual EF-hand and DLC-like domains. Given that the actions of calmodulin antagonists (such as CPZ and TFP), have been shown to be calcium-dependent, binding assays were performed under calcium-saturating conditions [60, 61]. Human UDP-galactose 4-epimerase (HsGALE), a dimeric enzyme which bears little structural similarity to EF-hand domain proteins, was used as a negative control [62, 63].

Limited proteolysis assays demonstrated that full-length SmTAL1 was partially protected from chymotrypsin proteolysis in the presence of PZQ, CPZ, W7 and TFP, and (possibly) in the presence of ThA (Figure 6). These effects were not observed in the presence of the drug-delivery vehicle, DMSO, nor were they observed in assays with the control protein, HsGALE, thereby confirming the specificity of SmTAL1-drug interactions (Figure 6). Although these data are broadly in agreement with previously reported differential scanning fluorimetry (DSF) assays, which demonstrated that SmTAL1 was stabilised in the presence of PZQ, CPZ, W7 and TFP, it should be noted that DSF assays did not detect a stabilising interaction in the presence of ThA [10]. It is possible that interactions with ThA are localised to a chymotrypsin cleavage site, since binding does not appear to affect the thermal stability of the protein.

Interestingly, limited proteolysis assays with the EF-hand fragment demonstrated partial protection from chymotrypsin proteolysis in the presence of W7, but not in the presence of the other drugs tested (implying that interactions with W7 are likely to be mediated by structural motifs within the EF-hand domain and/or linker region), whereas assays with the DLC fragment failed to display a digestion pattern in the presence of this protease (Figure 6). Dynein light chains form compact, stable structures and also form high affinity dimers; this may account for their relative resistance to proteolysis which has been observed in a number of previous studies [64-66]. Nevertheless, since drug interactions at the DLC-like domain could not be characterised using this method, the occurrence of a putative W7 binding site at the EF-hand domain, does not eliminate the possibility of an additional binding site at the DLC-like domain. Indeed, it should be noted that a previous study on FhCaBP2, demonstrated that both domains were partially protected from protease digestion in the presence of W7, implying the existence of multiple and/or overlapping binding sites for this drug [13].

SmTAL1 contains four tryptophan residues, one of which is positioned at the internal flanking helices of the EF-hand domain (Trp-49), and three of which are positioned within the DLC-like domain (Trp-152, Trp-162 and Trp-184). Thus, intrinsic fluorescence methodologies were also used to map putative

drug interactions to the individual functional domains. However, two of the drugs (W7 and TFP) could not be analysed using these methods, since their fluorescence emission spectra of these compounds partially overlapped with that of the protein (data not shown). SmTAL1 yielded a characteristic protein fluorescence emission spectrum, when incubated in the presence of calcium ions, and excited at 280 nm: a broad peak was observed, with a fluorescence intensity maximum (λ_{max}) at approximately 335 nm (Figure 6; Supplementary Table S2). When the full-length protein was treated with either CPZ or ThA, the fluorescence intensity at λ_{max} was significantly lower than that of the untreated protein; modest, but significant quenching was also observed with PZQ (Supplementary Table S2). These effects were not observed in the presence of the drug-delivery vehicle, DMSO, nor were they observed in assays with the control protein (the DLC-like domain from FhCaBP2, which has been previously shown not to interact with any of these drugs [13]). Thus, fluorescence quenching represents specific binding, rather than non-specific (collisional) contacts. It should be noted that λ_{max} was unchanged in these assays (Figure 6; Supplementary Table S2), suggesting that the hydrophobicity of the environment surrounding each Trp residue was not substantially altered upon drug binding [67]. Thus, quenching could be caused by protein-drug interactions, which occur within the vicinity of one (or more) tryptophan residue. Alternately, drug interactions may cause a structural change in SmTAL1, which affects the overall conformation of the full-length protein. In this scenario, the spatial repositioning of Trp resides, brings them into proximity to quenching groups, located within the protein matrix [67].

When the EF-hand domain fragment was treated with either CPZ or ThA, the fluorescence intensity at λ_{max} was significantly lower than that of the untreated protein; conversely, these effects were not observed in assays with the DLC-like domain (Figure 6; Supplementary Table S2). This indicates that interactions with CPZ and ThA are at least partially mediated by the EF-hand domain. Given that the only tryptophan residue in this domain (Trp-49) is positioned within the internal flanking helices of the EF-hand domain, these data are consistent with previous structural studies on CaM, which indicate that calmodulin antagonists bind to V-shaped, hydrophobic clefts formed by the internal flanking

helices [55, 68]. Interestingly, PZQ did not result in a statistically significant change in the fluorescence spectra of either the EF-hand domain or the DLC-like domain. It is possible that this drug binds between the two domains or that its effects (which are smaller than the other two drugs on the full-length protein) on the EF-hand domain are too small to be detected by this method.

It has previously been demonstrated using DSF that only one member of the SmTAL protein family (SmTAL1) undergoes a significant increase in thermal stability upon binding PZQ [10, 16]. To further investigate this, quantitative DSF was used to characterise the SmTAL1-PZQ interaction. As expected, SmTAL1 underwent a dose-dependent increase in thermal stability when incubated in the presence of a constant concentration of calcium ions, and titrated with PZQ, consistent with binding to the native, folded form of the protein, under the temperatures and conditions of the assay (Figure 7A-C) [51, 52]. Indeed, an initial plot of the titration data yielded a hyperbolic binding curve (Figure 7C,D), implying a simple, non-cooperative binding mechanism [53]. These data were fitted to both a non-cooperative (3PL) binding model, and a more complex (4PL) model with a variable Hill slope. There was no significant difference between 3PL and 4PL models ($P > 0.05$; F-test; $n = 3$) (Table 2), the simpler (3PL) model was chosen to fit the data. Thus, under these experimental conditions, Ca^{2+}-SmTAL1-PZQ complex formation was characterised by a non-cooperative binding scheme, with a 1:1 (protein: drug) stoichiometry, and an apparent dissociation constant ($K_{d,\,app}$) of approximately 140 µM (Table 2). PZQ has no detectable effect on the dimerization of SmTAL1 as measured by chemical crosslinking (Figure 7D,E).

3.6 SmTAL1 interacts with at least six compounds from the "Malaria Box"

The Medicines for Malaria Venture (MMV) provides an open-access set of 400 drug-like and probe-like compounds with activity against malarial parasites, termed the "Malaria Box". Although these compounds were primarily studied in the context of malaria research, numerous laboratories across the world have tested their potency and efficacy against an array of pathogenic species [38]. Thus, a

subset of the most potent compounds (including 40 drug-like, and 40 probe-like compounds from plate A; Table 3), were tested for their ability to bind SmTAL1 using a DSF assay. Hits were defined as those compounds that caused a significant change in the thermal stability of the protein *versus* the DMSO-only control.

Analysis of DSF screens demonstrated that the majority of Malaria box (plate A) compounds had no detectable effect on the thermal stability of SmTAL1 (Supplementary Table S4), with the exception of six probe-like compounds, designated A8, B10, D3, D11, E3 and G6 (Table 3; Supplementary Table S4). Five of these compounds (A8, D3, D11, E3 and G6) caused a significant increase in thermal stability *versus* the DMSO control (consistent with binding to the native, folded form of the protein), whereas one (B10), was shown to destabilise SmTAL1, suggesting preferential binding to a partially unfolded state (Table 3). Interestingly, a study undertaken by the Caffrey group (University of California, San Francisco), tested each of the 400 Malaria box compounds for their toxicity against newly transformed *S. mansoni* schistosomula. The effects of which were judged by visual inspection at 24, 48 and 72 hours-post-treatment. Those compounds that elicited the most profound effects were graded "4", whereas those that had no observable effect on the viability/ morphology of the worm were graded "0" (data accessed online at: doi: 10.6019/CHEMBL2363022) [69]. Given that one of the hits identified in our DSF screens with SmTAL1 (A8; 2-[[2-[2-Ethyl-2-methyl-4-(4-methylphenyl)oxan-4-yl]ethylamino]methyl]phenol), was shown to have a category 4 effect on juvenile worms, 72 hours-post-treatment, this compound would make an interesting candidate for future study (Table 4). Two further screens of the MMV compounds have been carried out by the Keiser group. It should be noted that none of the compounds demonstrated to bind SmTAL1 affected either juvenile or adult schistosomes in these screens, nor are they reported to have any effect on *F. hepatica* [70-72].

3.7 SmTAL1 interacts with an IQ-motif from the voltage-gated calcium channel, SmCa$_v$1B

Initial DSF screens demonstrated a putative interaction between SmTAL1 and SmIQ3, a 23-mer synthetic peptide derived from an IQ sequence, located in one of the parasite's voltage-gated calcium (Ca_V) channels, $SmCa_V1B$. No interactions were detected with other IQ-motifs derived from the parasite's voltage-gated calcium channels (data not shown; see Supplementary Table S3 for peptide sequences). This IQ-motif is the same one which we have recently shown interacts with two *S. mansoni* calmodulins (SmCaM1 and SmCaM2) [33]. This hints at the possibility of a physiologically relevant interaction between SmTAL1 the $SmCa_V1B$ calcium channel, and a possible role in calcium homeostasis. To investigate this, we undertook further DSF analyses and cross-linking assays.

SmTAL1 underwent a dose-dependent increase in thermal stability when incubated in the presence of calcium ions and titrated with the SmIQ3 peptide (Figure 8A-D), consistent with binding to the native, folded form of the protein, under the temperatures and conditions of the assay. Quantitative analyses of these data showed that they were best fit by the 4PL model, with a Hill slope of approximately 2 (Table 2).

Initial crosslinking assays with SmTAL1 indicated a differential response to the SmIQ3 peptide in the presence and absence of calcium ions. Thus, Ca^{2+}-SmTAL1 was titrated with SmIQ3 in the presence of a fixed concentration of BS^3, to evaluate whether this effect was concentration-dependent. As the concentration of SmIQ3 increased, both (monomer and dimer) bands were slightly retarded in mobility (Figure 8E). This could result from a gain in molecular mass, consistent with SmTAL1-SmIQ3 complex formation. Furthermore, it was noted that the density of the monomer band decreased with increasing peptide concentrations, while the SmTAL1 dimer band became darker, yet more dispersed (Figure 8E). Densitometric analysis of the monomer band, indicated that this was a saturatable, dose-dependent effect implying a specific, stoichiometric interaction with the peptide was responsible (Figure 8F). Quantitative analysis of these data yielded an EC_{50} value of 28 µM, similar to the apparent disassociation constant derived from DSF experiments (23 µM; Table 2). Thus, it is possible that SmIQ3 binding cooperatively promotes conformational change in the SmTAL1 dimer. It may also promote

increased conformational heterogeneity as evidenced by the dispersal of the band corresponding to the dimer (Figure 8E).

Given that PZQ is known to affect calcium homeostasis in the *Schistosoma spp.*, we hypothesised that the drug might affect the SmTAL1-SmIQ3 complex. In DSF assays, PZQ and the SmIQ3 peptide affected the thermal stability of the Ca^{2+}-SmTAL1 complex but did not abolish the effect (Figure 9). This suggested that SmIQ3 binding still occurred in the presence of saturating concentrations of PZQ. Presumably these two molecules bind at distinct, separate sites in SmTAL1.

To explore possible allosteric effects of PZQ on the Ca^{2+}-SmTAL1-SmIQ3 complex, semi-quantitative DSF was used to measure peptide-binding in the presence of this drug (Figure 9). Calcium-saturated Ca^{2+}-SmTAL1 was titrated with SmIQ3, either in the presence of the drug-delivery vehicle, DMSO (1 % v/v), or in the presence of PZQ, at a range of concentrations (20-500 µM) (Figure 9). The resulting data were fitted (globally) to a hyperbolic binding equation with a variable Hill slope and an extra-sum-of-squares F-test was used to gauge whether the parameters of the model differed between each dataset, with a null hypothesis that a single binding curve would adequately describe all datasets. Global analyses indicated that the shape of the binding curves was significantly altered with increasing concentrations of PZQ ($P < 0.0001$; F-test; $n = 3$). Therefore, to allow formal comparison between datasets (as inferred by changes in $K_{d,\ app}$ and ΔT_{max}), we determined whether the Hill slope (h) was significantly changed by PZQ addition, with a null hypothesis that a single value of h would adequately describe each binding curve. Since a single Hill slope of approximately 1.4 was sufficient to describe the entire family of binding curves ($P > 0.05$; F-test; $n = 3$), this parameter was constrained to allow estimation of $K_{d,\ app}$ and ΔT_{max}, (Table 4). This model generated an apparent dissociation constant of approximately 27 µM for the untreated Ca^{2+}-SmTAL1- SmIQ3 binding complex in the presence of DMSO (Table 4). This value was not significantly different ($P > 0.05$; F-test; $n = 3$) from the $K_{d,app}$ of the Ca^{2+}-SmTAL1- SmIQ3 complex in the absence of DMSO (~ 23 µM) (Table 2), demonstrating that the drug-delivery vehicle had no effect on the affinity. The dissociation constant of the Ca^{2+}-SmTAL1-

SmIQ3 binding complex was significantly decreased upon addition of PZQ (Table 4), suggesting that the strength of the protein-peptide interaction was enhanced approximately three-fold in the presence of saturating concentrations of this drug, implying a positive allosteric effect on protein-peptide interactions. However, it should be noted that there is no obvious pattern to the change in $K_{d,app}$. This suggests complex effects of the drug on this system.

3.8 Conclusions

Taken together, these results demonstrate that the SmTAL1 dimer exhibits complex, cooperative responses to binding partners. Each dimer has four functional calcium binding sites and there are cooperative interactions between these sites. SmTAL1 is able to interact with an IQ-motif from a voltage-gated calcium channel. This interaction is not directly antagonised by PZQ. In fact, this interaction is strengthened in the presence of the drug, although the precise relationship appears to be complex. Based on the data presented here, we propose that SmTAL1 may have a role in the regulation of at least one voltage-gated calcium channel in *S. mansoni.* Given that SmTAL1 reversibly interacts with calcium ions, it seems reasonable to assume that its role may be important in the calcium-dependent regulation of this channel. Such regulation is likely to require reversible interaction between the channel and the regulator. PZQ alters the affinity of this interaction and is, therefore, likely to disturb any regulatory mechanisms which are mediated by PZQ.

To demonstrate the significance of this postulated regulatory mechanism in the mechanism of action of PZQ, further experimental data will be required. Critically, it will be necessary to establish what role SmTAL1 (if any) has in the regulation of voltage-gated calcium channels. Assuming that it does have a role, then it should then be relatively straightforward to predict and test the consequences of increasing the affinity of the channel's interaction with SmTAL1. If this interaction represents a significant pharmacological target for PZQ, then we would expect it to be affected by structurally related compounds. Structure-activity relationships with PZQ derivatives on this interaction should

broadly match those already reported for effects on the intact parasite (e.g [73-79]). Furthermore, it would be expected that the pharmacologically active (*R*) enantiomer would have a greater effect on the interaction than the inactive (*S*) form.

It should also be stressed that, since several diverse proteins have been identified as PZQ binders, even if the interactions documented here prove to be important in the mechanism, they are unlikely to represent the only pharmacologically important action of PZQ. Recently, a transient receptor potential channel (SmTRPMPZQ; Smp_246790) has been identified as a likely pharmacological target of PZQ. The drug causes unregulated calcium ion influx through this channel [80, 81]. If this proves to be the main pharmacological target of PZQ, it will still be important to study voltage-gated calcium channels and their regulators. Other compounds which interact with SmTAL1 (e.g. the malaria box compounds in Table 3) may also interfere with the putative regulatory system proposed here and are thus likely to be promising leads for new anti-schistosomal drugs. It will also be interesting to see if SmTRPMPZQ interacts with any members of the SmTAL family.

Acknowledgements

CMT thanks the Department of Employment and Learning Northern Ireland (DELNI, UK) for a PhD studentship. We thank the Medicines Malaria Ventures foundation for providing the Malaria Box compounds.

CMT conducted and designed all experiments and statistical analyses. CMT and DJT analysed the data. DJT supervised CMT and drafted the paper based on initial drafts by CMT.

The authors have no conflicts of interest to declare

References

[1] C.M. Thomas, D.J. Timson, A mysterious family of calcium-binding proteins from parasitic worms, Biochem Soc Trans, 44 (2016) 1005-1010.
[2] S.L. Russell, D.J. Timson, Calcium binding proteins in the liver fluke, *Fasciola hepatica*, New Developments in Calcium Signaling Research, Nova Science Publishers, Inc2014, pp. 89-104.
[3] T.H. Nguyen, C.M. Thomas, D.J. Timson, M.J. van Raaij, *Fasciola hepatica* calcium-binding protein FhCaBP2: structure of the dynein light chain-like domain, Parasitol Res, 115 (2016) 2879-2886.
[4] Y.J. Kim, W.G. Yoo, M.R. Lee, J.M. Kang, B.K. Na, S.H. Cho, M.Y. Park, J.W. Ju, Molecular and Structural Characterization of the Tegumental 20.6-kDa Protein in *Clonorchis sinensis* as a Potential Druggable Target, Int J Mol Sci, 18 (2017) 557.
[5] C.H. Jo, J. Son, S. Kim, T. Oda, J. Kim, M.R. Lee, M. Sato, H.T. Kim, S. Unzai, S.Y. Park, K.Y. Hwang, Structural insights into a 20.8-kDa tegumental-allergen-like (TAL) protein from *Clonorchis sinensis*, Sci Rep, 7 (2017) 1764.
[6] Y.J. Kim, W.G. Yoo, M.R. Lee, D.W. Kim, W.J. Lee, J.M. Kang, B.K. Na, J.W. Ju, Identification and characterization of a novel 21.6-kDa tegumental protein from *Clonorchis sinensis*, Parasitol Res, 110 (2012) 2061-2066.
[7] G. Senawong, T. Laha, A. Loukas, P.J. Brindley, B. Sripa, Cloning, expression, and characterization of a novel *Opisthorchis viverrini* calcium-binding EF-hand protein, Parasitology international, 61 (2012) 94-100.
[8] P. Subpipattana, R. Grams, S. Vichasri-Grams, Analysis of a calcium-binding EF-hand protein family in *Fasciola gigantica*, Experimental parasitology, 130 (2012) 364-373.
[9] S. Vichasri-Grams, P. Subpipattana, P. Sobhon, V. Viyanant, R. Grams, An analysis of the calcium-binding protein 1 of *Fasciola gigantica* with a comparison to its homologs in the phylum Platyhelminthes, Molecular and biochemical parasitology, 146 (2006) 10-23.
[10] C.M. Thomas, C.M. Fitzsimmons, D.W. Dunne, D.J. Timson, Comparative biochemical analysis of three members of the *Schistosoma mansoni* TAL family: Differences in ion and drug binding properties, Biochimie, 108 (2015) 40-47.
[11] C.M. Fitzsimmons, F.M. Jones, A. Stearn, I.W. Chalmers, K.F. Hoffmann, J. Wawrzyniak, S. Wilson, N.B. Kabatereine, D.W. Dunne, The *Schistosoma mansoni* tegumental-allergen-like (TAL) protein family: influence of developmental expression on human IgE responses, PLoS neglected tropical diseases, 6 (2012) e1593.
[12] S. Cheung, C.M. Thomas, D.J. Timson, FhCaBP1 (FH22): A *Fasciola hepatica* calcium-binding protein with EF-hand and dynein light chain domains, Exp Parasitol, 170 (2016) 109-115.
[13] C.M. Thomas, D.J. Timson, FhCaBP2: a *Fasciola hepatica* calcium-binding protein with EF-hand and dynein light chain domains, Parasitology, 142 (2015) 1375-1386.
[14] S. Banford, O. Drysdale, E.M. Hoey, A. Trudgett, D.J. Timson, FhCaBP3: A *Fasciola hepatica* calcium binding protein with EF-hand and dynein light chain domains, Biochimie, 95 (2013) 751-758.
[15] R. Orr, R. Kinkead, R. Newman, L. Anderson, E.M. Hoey, A. Trudgett, D.J. Timson, FhCaBP4: a *Fasciola hepatica* calcium-binding protein with EF-hand and dynein light chain domains, Parasitology research, 111 (2012) 1707-1713.
[16] J. Carson, C.M. Thomas, A. McGinty, G. Takata, D.J. Timson, The tegumental allergen-like proteins of *Schistosoma mansoni*: A biochemical study of SmTAL4-TAL13, Mol Biochem Parasitol, 221 (2018) 14-22.
[17] J. Xu, Y. Ren, X. Xu, J. Chen, Y. Li, W. Gan, Z. Zhang, H. Zhan, X. Hu, *Schistosoma japonicum* tegumental protein 20.8, role in reproduction through its calcium binding ability, Parasitology research, 113 (2014) 491-497.
[18] M.M. Mohamed, K.A. Shalaby, P.T. LoVerde, A.M. Karim, Characterization of Sm20.8, a member of a family of schistosome tegumental antigens, Molecular and biochemical parasitology, 96 (1998) 15-25.

[19] S.A. Jeffs, P. Hagan, R. Allen, R. Correa-Oliveira, S.R. Smithers, A.J. Simpson, Molecular cloning and characterisation of the 22-kilodalton adult *Schistosoma mansoni* antigen recognised by antibodies from mice protectively vaccinated with isolated tegumental surface membranes, Molecular and biochemical parasitology, 46 (1991) 159-167.
[20] C.M. Fitzsimmons, T.J. Stewart, K.F. Hoffmann, J.L. Grogan, M. Yazdanbakhsh, D.W. Dunne, Human IgE response to the *Schistosoma haematobium* 22.6 kDa antigen, Parasite immunology, 26 (2004) 371-376.
[21] C.M. Fitzsimmons, R. McBeath, S. Joseph, F.M. Jones, K. Walter, K.F. Hoffmann, H.C. Kariuki, J.K. Mwatha, G. Kimani, N.B. Kabatereine, B.J. Vennervald, J.H. Ouma, D.W. Dunne, Factors affecting human IgE and IgG responses to allergen-like *Schistosoma mansoni* antigens: Molecular structure and patterns of in vivo exposure, International archives of allergy and immunology, 142 (2007) 40-50.
[22] K.F. Hoffmann, M. Strand, Molecular characterization of a 20.8-kDa *Schistosoma mansoni* antigen. Sequence similarity to tegumental associated antigens and dynein light chains, The Journal of biological chemistry, 272 (1997) 14509-14515.
[23] C.M. Thomas, D.J. Timson, The Mechanism of Action of Praziquantel: Six Hypotheses, Curr Top Med Chem, 18 (2018) 1575-1584.
[24] N. Vale, M.J. Gouveia, G. Rinaldi, P.J. Brindley, F. Gartner, J.M. Correia da Costa, Praziquantel for Schistosomiasis: Single-Drug Metabolism Revisited, Mode of Action, and Resistance, Antimicrob Agents Chemother, 61 (2017).
[25] V.B.R. da Silva, B. Campos, J.F. de Oliveira, J.L. Decout, M. do Carmo Alves de Lima, Medicinal chemistry of antischistosomal drugs: Praziquantel and oxamniquine, Bioorg Med Chem, 25 (2017) 3259-3277.
[26] R.M. Greenberg, Are Ca^{2+} channels targets of praziquantel action?, International journal for parasitology, 35 (2005) 1-9.
[27] E.Y. Seto, B.K. Wong, D. Lu, B. Zhong, Human schistosomiasis resistance to praziquantel in China: should we be worried?, Am J Trop Med Hyg, 85 (2011) 74-82.
[28] F.F. Couto, P.M. Coelho, N. Araujo, J.R. Kusel, N. Katz, L.K. Jannotti-Passos, A.C. Mattos, *Schistosoma mansoni*: a method for inducing resistance to praziquantel using infected *Biomphalaria glabrata* snails, Mem Inst Oswaldo Cruz, 106 (2011) 153-157.
[29] R.S. Kasinathan, W.M. Morgan, R.M. Greenberg, *Schistosoma mansoni* express higher levels of multidrug resistance-associated protein 1 (SmMRP1) in juvenile worms and in response to praziquantel, Mol Biochem Parasitol, 173 (2010) 25-31.
[30] L. Pica-Mattoccia, M.J. Doenhoff, C. Valle, A. Basso, A.R. Troiani, P. Liberti, A. Festucci, A. Guidi, D. Cioli, Genetic analysis of decreased praziquantel sensitivity in a laboratory strain of *Schistosoma mansoni*, Acta Trop, 111 (2009) 82-85.
[31] W. Wang, B.A. Malcolm, Two-stage PCR protocol allowing introduction of multiple mutations, deletions and insertions using QuikChange Site-Directed Mutagenesis, BioTechniques, 26 (1999) 680-682.
[32] L. Ornstein, B.J. Davis, Disc electrophoresis-I: Background and theory, Ann NY Acad Sci, 121 (1964) 321-349.
[33] C.M. Thomas, D.J. Timson, Calmodulins from *Schistosoma mansoni*: biochemical analysis and interaction with IQ-motifs from voltage-gated calcium channels., Cell Calcium, 74 (2018) 1-13.
[34] M. McAuley, M. Huang, D.J. Timson, Insight into the mechanism of galactokinase: Role of a critical glutamate residue and helix/coil transitions, Biochim Biophys Acta, 1865 (2017) 321-328.
[35] D.J. Timson, R.J. Reece, Functional analysis of disease-causing mutations in human galactokinase, European journal of biochemistry / FEBS, 270 (2003) 1767-1774.
[36] M.D. Partis, D.G. Griffiths, G.C. Roberts, R.D. Beechey, Cross-linking of protein by ω-maleimido alkanoyl N-hydroxysuccinimido esters, Journal of Protein Chemistry, 2 (1983) 263-277.
[37] D.J. Timson, Functional analysis of disease-causing mutations in human UDP-galactose 4-epimerase, FEBS J., 272 (2005) 6170-6177.

[38] W.C. Van Voorhis, J.H. Adams, R. Adelfio, V. Ahyong, M.H. Akabas, P. Alano, A. Alday, Y. Aleman Resto, A. Alsibaee, A. Alzualde, K.T. Andrews, S.V. Avery, V.M. Avery, L. Ayong, M. Baker, S. Baker, C. Ben Mamoun, S. Bhatia, Q. Bickle, L. Bounaadja, T. Bowling, J. Bosch, L.E. Boucher, F.F. Boyom, J. Brea, M. Brennan, A. Burton, C.R. Caffrey, G. Camarda, M. Carrasquilla, D. Carter, M. Belen Cassera, K. Chih-Chien Cheng, W. Chindaudomsate, A. Chubb, B.L. Colon, D.D. Colon-Lopez, Y. Corbett, G.J. Crowther, N. Cowan, S. D'Alessandro, N. Le Dang, M. Delves, J.L. DeRisi, A.Y. Du, S. Duffy, S. Abd El-Salam El-Sayed, M.T. Ferdig, J.A. Fernandez Robledo, D.A. Fidock, I. Florent, P.V. Fokou, A. Galstian, F.J. Gamo, S. Gokool, B. Gold, T. Golub, G.M. Goldgof, R. Guha, W.A. Guiguemde, N. Gural, R.K. Guy, M.A. Hansen, K.K. Hanson, A. Hemphill, R. Hooft van Huijsduijnen, T. Horii, P. Horrocks, T.B. Hughes, C. Huston, I. Igarashi, K. Ingram-Sieber, M.A. Itoe, A. Jadhav, A. Naranuntarat Jensen, L.T. Jensen, R.H. Jiang, A. Kaiser, J. Keiser, T. Ketas, S. Kicka, S. Kim, K. Kirk, V.P. Kumar, D.E. Kyle, M.J. Lafuente, S. Landfear, N. Lee, S. Lee, A.M. Lehane, F. Li, D. Little, L. Liu, M. Llinas, M.I. Loza, A. Lubar, L. Lucantoni, I. Lucet, L. Maes, D. Mancama, N.R. Mansour, S. March, S. McGowan, I. Medina Vera, S. Meister, L. Mercer, J. Mestres, A.N. Mfopa, R.N. Misra, S. Moon, J.P. Moore, F. Morais Rodrigues da Costa, J. Muller, A. Muriana, S. Nakazawa Hewitt, B. Nare, C. Nathan, N. Narraidoo, S. Nawaratna, K.K. Ojo, D. Ortiz, G. Panic, G. Papadatos, S. Parapini, K. Patra, N. Pham, S. Prats, D.M. Plouffe, S.A. Poulsen, A. Pradhan, C. Quevedo, R.J. Quinn, C.A. Rice, M. Abdo Rizk, A. Ruecker, R. St Onge, R. Salgado Ferreira, J. Samra, N.G. Robinett, U. Schlecht, M. Schmitt, F. Silva Villela, F. Silvestrini, R. Sinden, D.A. Smith, T. Soldati, A. Spitzmuller, S.M. Stamm, D.J. Sullivan, W. Sullivan, S. Suresh, B.M. Suzuki, Y. Suzuki, S.J. Swamidass, D. Taramelli, L.R. Tchokouaha, A. Theron, D. Thomas, K.F. Tonissen, S. Townson, A.K. Tripathi, V. Trofimov, K.O. Udenze, I. Ullah, C. Vallieres, E. Vigil, J.M. Vinetz, P. Voong Vinh, H. Vu, N.A. Watanabe, K. Weatherby, P.M. White, A.F. Wilks, E.A. Winzeler, E. Wojcik, M. Wree, W. Wu, N. Yokoyama, P.H. Zollo, N. Abla, B. Blasco, J. Burrows, B. Laleu, D. Leroy, T. Spangenberg, T. Wells, P.A. Willis, Open Source Drug Discovery with the Malaria Box Compound Collection for Neglected Diseases and Beyond, PLoS Pathog, 12 (2016) e1005763.

[39] T. Spangenberg, J.N. Burrows, P. Kowalczyk, S. McDonald, T.N. Wells, P. Willis, The open access malaria box: a drug discovery catalyst for neglected diseases, PLoS One, 8 (2013) e62906.

[40] C.M. Moore, E.M. Hoey, A. Trudgett, D.J. Timson, A plasma membrane Ca^{2+}-ATPase (PMCA) from the liver fluke, *Fasciola hepatica*, International journal for parasitology, 42 (2012) 851-858.

[41] E. Atcheson, E. Hamilton, S. Pathmanathan, B. Greer, P. Harriott, D.J. Timson, IQ-motif selectivity in human IQGAP2 and IQGAP3:binding of calmodulin and myosin essential light chain, Bioscience Reports, 31 (2011) 371-379.

[42] S. Pathmanathan, S.F. Elliott, S. McSwiggen, B. Greer, P. Harriott, G.B. Irvine, D.J. Timson, IQ motif selectivity in human IQGAP1: binding of myosin essential light chain and S100B, Molecular and cellular biochemistry, 318 (2008) 43-51.

[43] M.M. Bradford, A rapid and sensitive method for the quantitation of microgram quantities of protein utilizing the principle of protein-dye binding, Analytical Biochemistry, 72 (1976) 248-254.

[44] T.J. Schoenmakers, G.J. Visser, G. Flik, A.P. Theuvenet, CHELATOR: an improved method for computing metal ion concentrations in physiological solutions, Biotechniques, 12 (1992) 870-874, 876-879.

[45] D.M. Bers, C.W. Patton, R. Nuccitelli, A practical guide to the preparation of Ca^{2+} buffers, Methods Cell Biol, 40 (1994) 3-29.

[46] J.L. Gifford, M.P. Walsh, H.J. Vogel, Structures and metal-ion-binding properties of the Ca^{2+}-binding helix-loop-helix EF-hand motifs, The Biochemical journal, 405 (2007) 199-221.

[47] A. Malmendal, S. Linse, J. Evenas, S. Forsen, T. Drakenberg, Battle for the EF-hands: magnesium-calcium interference in calmodulin, Biochemistry, 38 (1999) 11844-11850.

[48] B. Wimberly, E. Thulin, W.J. Chazin, Characterization of the N-terminal half-saturated state of calbindin D9k: NMR studies of the N56A mutant, Protein Sci, 4 (1995) 1045-1055.

[49] K. Denessiouk, S. Permyakov, A. Denesyuk, E. Permyakov, M.S. Johnson, Two structural motifs within canonical EF-hand calcium-binding domains identify five different classes of calcium buffers and sensors, PLoS One, 9 (2014) e109287.

[50] D.C. LaPorte, B.M. Wierman, D.R. Storm, Calcium-induced exposure of a hydrophobic surface on calmodulin, Biochemistry, 19 (1980) 3814-3819.
[51] D. Matulis, J.K. Kranz, F.R. Salemme, M.J. Todd, Thermodynamic stability of carbonic anhydrase: measurements of binding affinity and stoichiometry using ThermoFluor, Biochemistry, 44 (2005) 5258-5266.
[52] M.D. Cummings, M.A. Farnum, M.I. Nelen, Universal screening methods and applications of ThermoFluor, Journal of biomolecular screening, 11 (2006) 854-863.
[53] K.D. Wilkinson, Quantitative analysis of protein-protein interactions, Methods Mol Biol, 261 (2004) 15-32.
[54] H. Abeliovich, An empirical extremum principle for the hill coefficient in ligand-protein interactions showing negative cooperativity, Biophysical journal, 89 (2005) 76-79.
[55] W.J. Cook, L.J. Walter, M.R. Walter, Drug binding by calmodulin: crystal structure of a calmodulin-trifluoperazine complex, Biochemistry, 33 (1994) 15259-15265.
[56] M. Vandonselaar, R.A. Hickie, J.W. Quail, L.T. Delbaere, Trifluoperazine-induced conformational change in Ca^{2+}-calmodulin, Nature structural biology, 1 (1994) 795-801.
[57] B.G. Vertessy, V. Harmat, Z. Bocskei, G. Naray-Szabo, F. Orosz, J. Ovadi, Simultaneous binding of drugs with different chemical structures to Ca^{2+}-calmodulin: crystallographic and spectroscopic studies, Biochemistry, 37 (1998) 15300-15310.
[58] M. Humar, S.E. Pischke, T. Loop, A. Hoetzel, R. Schmidt, C. Klaas, H.L. Pahl, K.K. Geiger, B.H. Pannen, Barbiturates directly inhibit the calmodulin/calcineurin complex: a novel mechanism of inhibition of nuclear factor of activated T cells, Molecular pharmacology, 65 (2004) 350-361.
[59] M. Gnanasekar, A.M. Salunkhe, A.K. Mallia, Y.X. He, R. Kalyanasundaram, Praziquantel affects the regulatory myosin light chain of *Schistosoma mansoni*, Antimicrobial Agents and Chemotherapy, 53 (2009) 1054-1060.
[60] D.R. Marshak, T.J. Lukas, D.M. Watterson, Drug-protein interactions: binding of chlorpromazine to calmodulin, calmodulin fragments, and related calcium binding proteins, Biochemistry, 24 (1985) 144-150.
[61] L. Massom, H. Lee, H.W. Jarrett, Trifluoperazine binding to porcine brain calmodulin and skeletal muscle troponin C, Biochemistry, 29 (1990) 671-681.
[62] J.B. Thoden, T.M. Wohlers, J.L. Fridovich-Keil, H.M. Holden, Crystallographic evidence for Tyr 157 functioning as the active site base in human UDP-galactose 4-epimerase, Biochemistry (John Wiley & Sons), 39 (2000) 5691-5701.
[63] T.J. McCorvie, D.J. Timson, UDP-galactose 4-epimerase (GALE), in: N. Taniguchi, K. Honke, M. Fukuda, H. Narimatsu, Y. Yamaguchi, T. Angata (Eds.) Handbook of Glycosyltransferases and Related Genes, Springer, New York, 2014, pp. Chapter 133.
[64] M. Makokha, M. Hare, M. Li, T. Hays, E. Barbar, Interactions of cytoplasmic dynein light chains Tctex-1 and LC8 with the intermediate chain IC74, Biochemistry, 41 (2002) 4302-4311.
[65] A. Nyarko, M. Hare, M. Makokha, E. Barbar, Interactions of LC8 with N-terminal segments of the intermediate chain of cytoplasmic dynein, ScientificWorldJournal, 3 (2003) 647-654.
[66] L. Wang, M. Hare, T.S. Hays, E. Barbar, Dynein light chain LC8 promotes assembly of the coiled-coil domain of swallow protein, Biochemistry, 43 (2004) 4611-4620.
[67] J.R. Lakowicz, Principles of Fluorescence Spectroscopy, Springer US, New York, 2006.
[68] M. Osawa, M.B. Swindells, J. Tanikawa, T. Tanaka, T. Mase, T. Furuya, M. Ikura, Solution structure of calmodulin-W-7 complex: the basis of diversity in molecular recognition, Journal of Molecular Biology, 276 (1998) 165-176.
[69] M.H. Abdulla, D.S. Ruelas, B. Wolff, J. Snedecor, K.C. Lim, F. Xu, A.R. Renslo, J. Williams, J.H. McKerrow, C.R. Caffrey, Drug discovery for schistosomiasis: hit and lead compounds identified in a library of known drugs by medium-throughput phenotypic screening, PLoS Negl Trop Dis, 3 (2009) e478.
[70] V. Pasche, B. Laleu, J. Keiser, Screening a repurposing library, the Medicines for Malaria Venture Stasis Box, against Schistosoma mansoni, Parasit Vectors, 11 (2018) 298.

[71] K. Ingram-Sieber, N. Cowan, G. Panic, M. Vargas, N.R. Mansour, Q.D. Bickle, T.N. Wells, T. Spangenberg, J. Keiser, Orally active antischistosomal early leads identified from the open access malaria box, PLoS Negl Trop Dis, 8 (2014) e2610.
[72] C. Machicado, M.P. Soto, O. Timoteo, A. Vaisberg, M. Pajuelo, P. Ortiz, L.A. Marcos, Screening the Pathogen Box for Identification of New Chemical Agents with Anti-Fasciola hepatica Activity, Antimicrob Agents Chemother, 63 (2019).
[73] W.W. Duan, S.J. Qiu, Y. Zhao, H. Sun, C. Qiao, C.M. Xia, Praziquantel derivatives exhibit activity against both juvenile and adult *Schistosoma japonicum*, Bioorg Med Chem Lett, 22 (2012) 1587-1590.
[74] F. Ronketti, A.V. Ramana, X. Chao-Ming, L. Pica-Mattoccia, D. Cioli, M.H. Todd, Praziquantel derivatives I: Modification of the aromatic ring, Bioorg Med Chem Lett, 17 (2007) 4154-4157.
[75] Z.X. Wang, J.L. Chen, C. Qiao, Praziquantel derivatives with antischistosomal activity: aromatic ring modification, Chem Biol Drug Des, 82 (2013) 216-225.
[76] J.J. Yang, J. Boissier, J.L. Chen, H. Yao, S. Yang, A. Rognon, C. Qiao, Design, synthesis and biological evaluation of praziquantel and endoperoxide conjugates as antischistosomal agents, Future Med Chem, 7 (2015) 713-725.
[77] W.L. Wang, L.J. Song, X. Chen, X.R. Yin, W.H. Fan, G.P. Wang, C.X. Yu, B. Feng, Synthesis and SAR studies of praziquantel derivatives with activity against Schistosoma japonicum, Molecules, 18 (2013) 9163-9178.
[78] S. Guglielmo, D. Cortese, F. Vottero, B. Rolando, V.P. Kommer, D.L. Williams, R. Fruttero, A. Gasco, New praziquantel derivatives containing NO-donor furoxans and related furazans as active agents against Schistosoma mansoni, Eur J Med Chem, 84 (2014) 135-145.
[79] Y. Zheng, L. Dong, C. Hu, B. Zhao, C. Yang, C. Xia, D. Sun, Development of chiral praziquantel analogues as potential drug candidates with activity to juvenile Schistosoma japonicum, Bioorg Med Chem Lett, 24 (2014) 4223-4226.
[80] S.K. Park, G.S. Gunaratne, E.G. Chulkov, F. Moehring, P. McCusker, P.I. Dosa, J.D. Chan, C.L. Stucky, J.S. Marchant, The anthelmintic drug praziquantel activates a schistosome transient receptor potential channel, J Biol Chem, (2019).
[81] S.K. Park, J.S. Marchant, The Journey to Discovering a Flatworm Target of Praziquantel: A Long TRP, Trends Parasitol, (2019).
[82] K.L. Blair, J.L. Bennett, R.A. Pax, Praziquantel: physiological evidence for its site(s) of action in magnesium-paralysed *Schistosoma mansoni*, Parasitology, 104 Pt 1 (1992) 59-66.

Figure Legends

Figure 1: **Structure and sequence of SmTAL1**. (A) Modelled structure of SmTAL1 with the EF-hand domain and linker region shown in red (corresponding to the EF-hand fragments used in this paper) and the DLC-like domain in blue (corresponding to the DLC-like fragments used in this paper). (B) Protein sequence of SmTAL1 shown in the same colour scheme as the structure. Residues altered to disrupt calcium binding in the EF-hands are highlighted in yellow (EF1) and green (EF2).

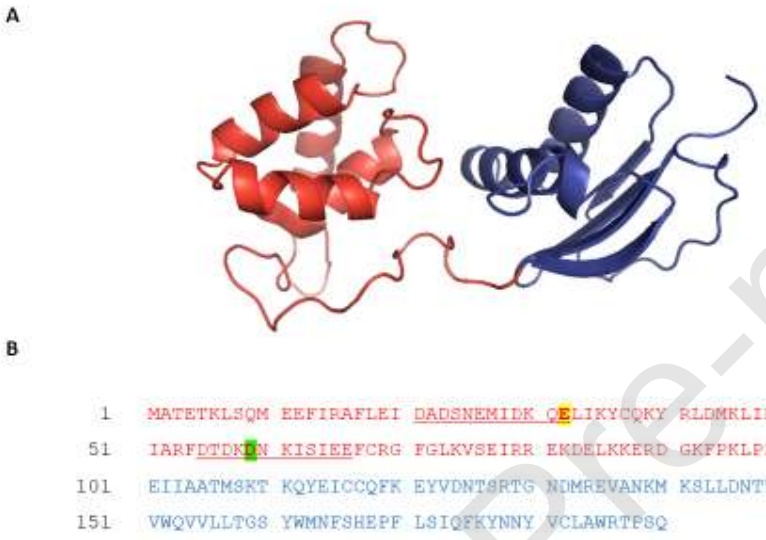

Figure 2: **Ion binding by SmTAL1, SmTAL1 domains and variants, as revealed by native-PAGE.** Wild-type SmTAL1, SmTAL1-E32A and SmTAL1-D59A (19 µM), fragments corresponding the wild-type EF-hand domain, EF-E32A and EF-D59A (21 µM), and the DLC-like domain (9 µM), were incubated in the presence of EGTA (1 mM), or EGTA (1 mM) and the appropriate ion solution (2 mM), and resolved on 6 % discontinuous native-PAGE at pH 8.3 [32]. U, untreated protein; E, EGTA treated protein; ion treatment groups are indicated by panels. The gel image in the blue box represents a comparison between the wild-type EF-hand domain, and the EF-E32A variant. The wild-type EF-hand domain is shown on the left of the dashed line and the EF-E32A variant to the right.

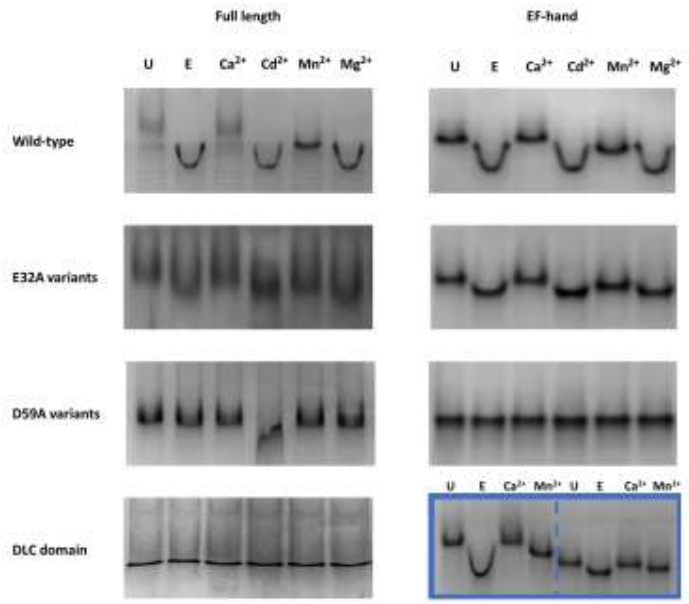

Figure 3: **Ion binding by SmTAL1, SmTAL1 domains and variants, as revealed by ANS fluorescence.** Wild-type SmTAL1, EF-hand domain, DLC-like domain and variants, EF-E32A and EF-D99A (15 µM) were incubated either in the presence of EGTA (1 mM), or in the presence of EGTA (1 mM), and the appropriate ion solution (2 mM), then treated with ANS (36 µM). U, untreated protein samples are depicted in blue; E, EGTA treatment groups are depicted in red; ion treatment groups are depicted as follows: calcium (green), manganese (purple), and magnesium (orange). Fluorescence spectra are plots of the mean (n=3) fluorescence intensity, measured in arbitrary units (AU), over a range of emission wavelengths. Assays were baseline corrected using an equal volume of buffer, containing the appropriate concentration of EGTA/ion solution. Images were constructed in GraphPad Prism 6.0. Statistical significance was determined for each ion treatment group, and the untreated (U) protein sample *versus* the EGTA treatment group. Calculations were performed in GraphPad Prism 6.0, using one-way analysis of variance (ANOVA) followed by Tukey's post hoc test for multiple comparisons. Statistical significance is denoted as follows: not significant (ns) $P > 0{\cdot}05$; * $P \leq 0.05$; ** $P \leq 0.01$; **** $P \leq 0{\cdot}0001$. See, also, Supplementary Table S1.

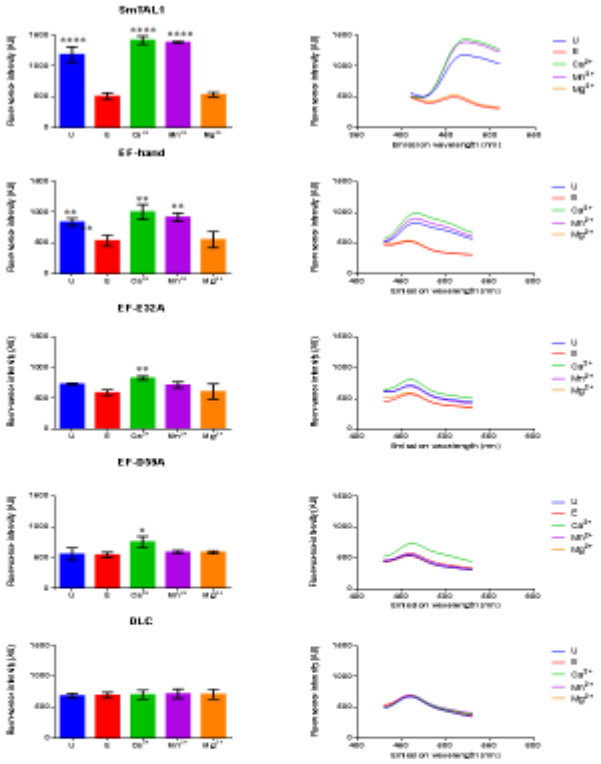

Figure 4: **Calcium binding by SmTAL1, SmTAL1-E32A and SmTAL1-D59A, as revealed by differential scanning fluorimetry.** Semi log plots (left) show the change in melting temperature (ΔT_m) as a function of concentration of free calcium ions ($[Ca^{2+}]_{free}$). The lines show the best fit following analysis by non-linear regression in in GraphPad Prism 6.0. Scatchard plots (right), were used as a visual aid to illustrate cooperativity. Concave-down indicates positive cooperativity, an intercept at the y-axis can indicate protein instability.

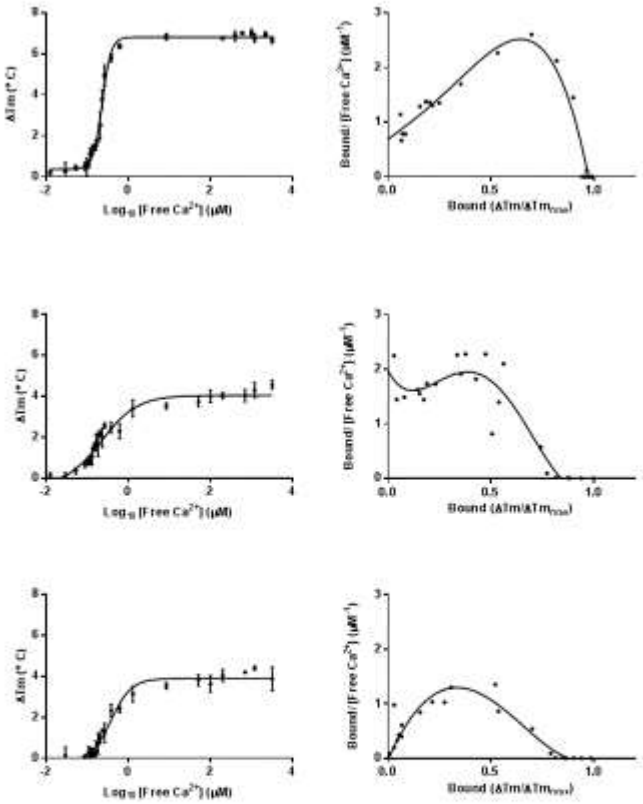

Figure 5: **Dimerisation of the SmTAL1 EF-hand and DLC-like domains, as revealed by crosslinking with BS^3.** The SmTAL1 EF-hand domain (40 µM), DLC-like domain (19 µM), and EF-hand domain variants, EF-E32A (27 µM), and EF-D59A (34 µM), were incubated in the presence of either EGTA (1 mM), or EGTA (1 mM) and the appropriate ion solution (2 mM), before treatment with the chemical crosslinker, BS^3 (700 µM), and resolved on 15 % SDS-PAGE. M, molecular mass marker (in kDa); U, untreated protein; (+), treated with BS^3; (-), not treated with BS^3. Monomers are indicated by (× 1), and dimers by (× 2).

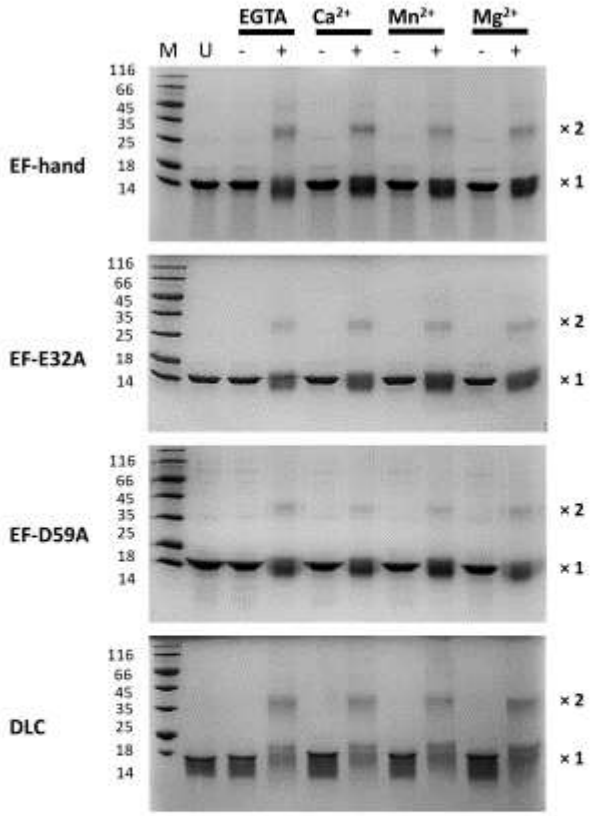

Figure 6: **Drug binding by SmTAL1, as revealed by limited proteolysis and intrinsic fluorescence.** Left panels: Full-length SmTAL1 (14 µM) and fragments corresponding to the SmTAL1 EF-hand domain (20 µM), and DLC-like domain (7.6 µM), were treated with calcium chloride (0.8 mM), and incubated in the presence of various drugs (250 µM). Chymotrypsin was added to each treatment group (at a final concentration of 600 nM in assays with SmTAL1, or 700 nM, in assays with protein fragments), and the resulting digestion patterns analysed by 15 % SDS-PAGE. M, molecular mass marker (in kDa); U, untreated protein; +, protein in the presence of chymotrypsin; D, DMSO control (1% v/v); P, PZQ; C,

CPZ; W, W7; T, TFP; ThA, thiamylal. All drugs all contained 1% (v/v) DMSO. DLC-like domain monomers are indicated by (× 1), and dimers by (× 2). Similar assays were conducted with control protein, human UDP-galactose 4-epimerase (HsGALE). Centre and right panels: SmTAL1, EF-hand and DLC-like domain fragments (10 µM) were incubated in the presence of calcium chloride (1 mM), and various drugs (100 µM). U, untreated protein samples are depicted in blue; D, DMSO control (1 % v/v) is depicted in red; drug treatment groups are depicted as follows: PZQ (green), CPZ (purple), thiamylal (ThA) (orange). Assays with the FhCaBP2-DLC-like domain control protein utilised similar conditions, apart from increased drug concentrations (250 µM). Bar charts (left) represent mean fluorescence intensity at λ_{max} (335 nm), when excited at 280 nm; error bars represent standard deviation from three repeat experiments. Fluorescence spectra (right) plot the mean fluorescence intensity, measured in arbitrary units (AU), over a range of emission wavelengths. Assays were baseline corrected using an equal volume of buffer, containing the appropriate concentration of drug. Images were constructed in GraphPad Prism.

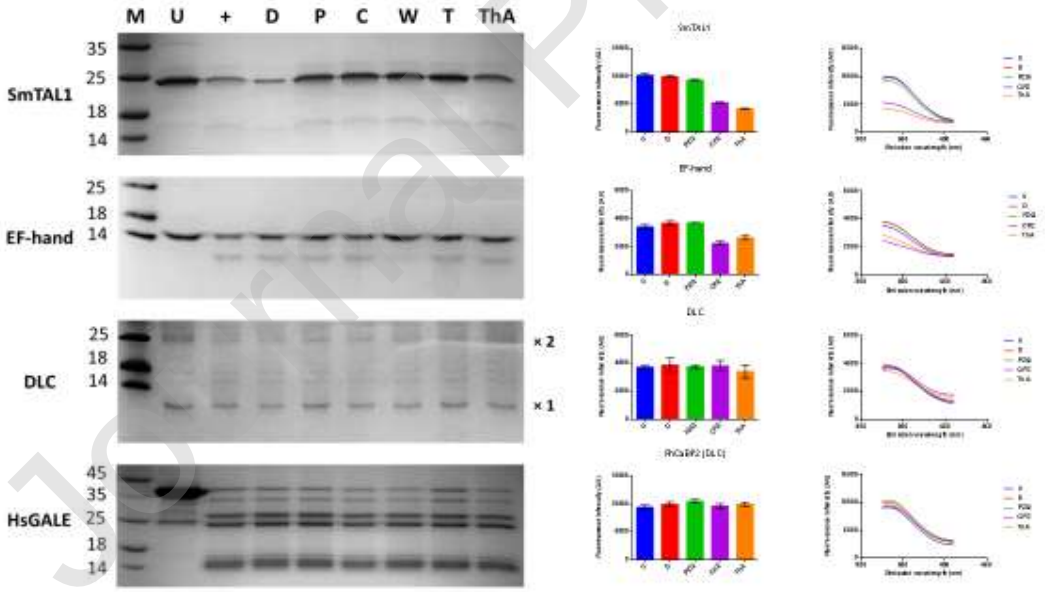

Figure 7: **PZQ binding by SmTAL1, as revealed by differential scanning fluorimetry and chemical crosslinking with BS^3.** (A) The bar chart shows the increase in thermal stability of SmTAL1 (10 µM), in

the presence of EGTA (1 mM) and calcium chloride (2 mM), when titrated with PZQ (10 data points, spanning 0.1 to 1.0 mM). U, untreated SmTAL1 shown in blue; D, DMSO (1 % v/v) vehicle-only control. The DMSO control was used as the zero PZQ group for titration data; Untreated and DMSO groups were not significantly different ($P > 0.05$; ANOVA; n = 3). Error bars represent the standard deviations of three repeat experiments. (B) Representative first differential traces showing the "melting point" (T_m) (^oC), at each step in the titration. (C) The change in melting temperatures (ΔT_m) was plotted against the concentration of SmIQ3 at each titration point. (D) Semi log plots in which ΔT_m (^oC) was plotted against the $\log_{10}$ ([PZQ]/M), and analysed by non-linear regression. (E, F) Gel images showing the crosslinking of SmTAL1 (10 µM) was incubated in the presence of 1 mM EGTA (E), or 1 mM EGTA and 2 mM calcium chloride (F), and treated with increasing concentrations of PZQ (5 data points, spanning 100 to 500 µM; as indicated by the black arrow). All samples (apart from U) were treated with the chemical crosslinker, BS^3 (800 µM). Protein bands were resolved on 15 % SDS-PAGE. M, molecular mass marker (in kDa); U, untreated protein; (+), treated with BS^3, but not PZQ; D, treated with DMSO (1 % v/v), but not PZQ. Monomers are indicated by (× 1), and dimers by (× 2).

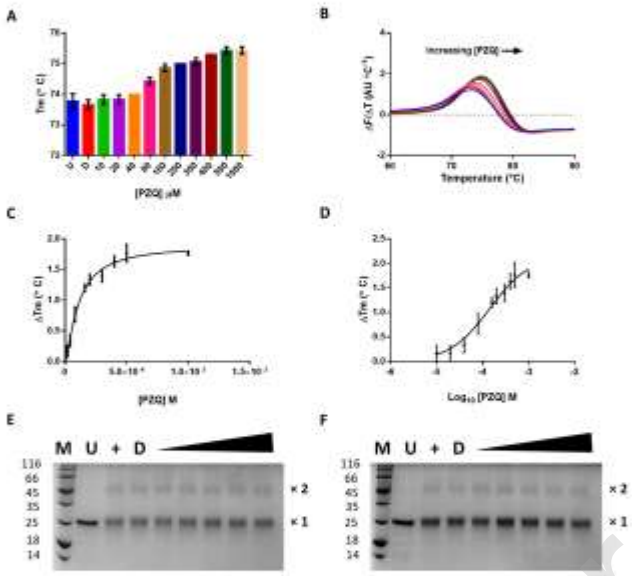

Figure 8: **SmIQ3 peptide binding by SmTAL1, as revealed by differential scanning fluorimetry and chemical crosslinking with BS^3.** (A) The bar chart shows increase in thermal stability of SmTAL1 (10 µM), in the presence of EGTA (1 mM) and calcium chloride (2 mM), when titrated with rising concentrations of peptide, SmIQ3 (10 data points, 1-160 µM). U, untreated SmTAL1 shown in blue. Error bars represent the standard deviation from three repeat experiments. (B) Representative first differential traces show the "melting point" (T_m), at each step in the titration. (C) The change in melting temperatures, ΔT_m, was plotted against the concentration of SmIQ3 at each titration point (D)

Klotz/semi log plots: ΔT_m (^oC) was plotted against the $\log_{10}$ [SmIQ3] (µM), and analysed by non-linear regression in in GraphPad Prism 6.0. (E) Gel image of SmTAL1 (10 µM) was incubated in the presence of EGTA (1 mM), calcium chloride (2 mM), and treated with rising concentrations of SmIQ3 (5 data points, spanning 10 to 160 µM; as indicated by the black arrow). All samples (apart from U) were treated with the chemical crosslinker, BS^3 (800 µM). Protein bands were resolved on 15 % SDS-PAGE. M, molecular mass marker (in kDa); U, untreated protein; (+), treated with BS^3, but no peptide. Monomers are indicated by (× 1), and dimers by (× 2). (F) The change in density (Δ density) of the monomer band was plotted against SmIQ3 concentration and fitted to equation 1 (where the half-maximal effect (EC_{50}) is defined by [SmIQ3] at Y_{mid}.

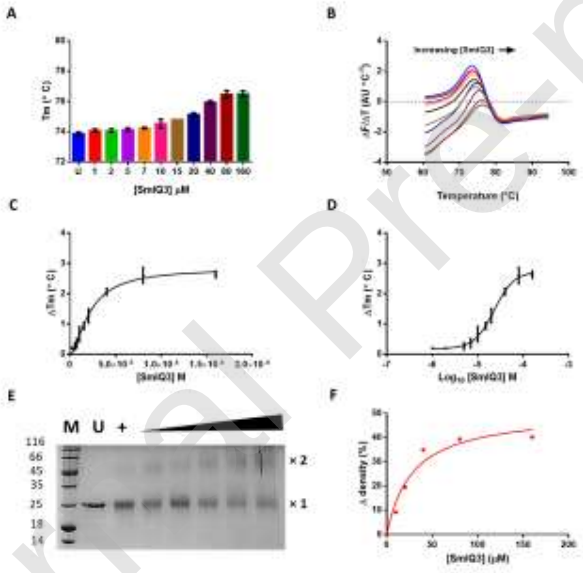

Figure 9: **SmIQ3 peptide binding by Ca^{2+}-SmTAL in the presence of rising concentrations of PZQ, as revealed by differential scanning fluorimetry.** A global fit was used to analyse the binding data from six SmIQ3 titrations (seven data points, spanning 5-80 µM), conducted in the presence of various, fixed concentrations of PZQ (six datasets, spanning 20-500 µM). Curve fitting was performed in GraphPad Prism 6.0, using titration data from DMSO-treated Ca^{2+}-SmTAL1 as the untreated group. Error bars represent the standard error from three repeat experiments. Please note that for the purposes of

clarity, the DMSO-only binding curve has been omitted from this graph. Arrow denotes rising concentrations of PZQ.

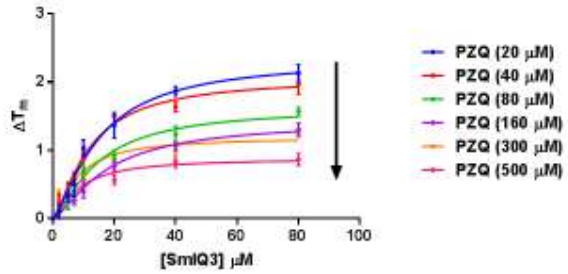

Tables

Table 1: **Calcium binding data for SmTAL1, SmTAL1-E32A and SmTAL1-D59A, as revealed by differential scanning fluorimetry**

	Protein		
	SmTAL1	**SmTAL1-E32A**	**SmTAL1-D59A**
Semi log plot Y_{max}	Sigmoidal (steep) 6.81	Sigmoidal 4.05	Sigmoidal 3.89
Best fit *R-square* *F-test*	4PL 0.99 ****	3PL 0.94 *Ns*	4PL 0.95 ****
$K_{d,\ app}$ (µM)	0.23 ± 0.00	0.23 ± 0.03^{ns}	0.38 ± 0.03 **
Hill slope	3.99 ± 0.27	1.0 (by definition)	1.75 ± 0.22
Scatchard *Est. cooperativity*	Concave-down Positive	Possible instability None	Concave-down Positive
Maximum coop sites	4	0	2
Oligomeric state	Dimer	Dimer	Dimer

Corrected binding data were optimised against a three-parameter (3PL) model or four-parameter model (4PL), by non-linear regression. The model that represented the best fit to the data was chosen (as judged by the R-square value, and the extra-sum-of-squares, F-test). If 3PL and 4PL models were not significantly different, the simpler model was chosen. The apparent dissociation constant ($K_{d,\ app}$), and Hill slope (h) were then derived from the plots. $K_{d,\ app}$ values were analysed by one-way analysis of variance (ANOVA) in GraphPad Prism 6.0, followed by Tukey's post hoc test for multiple comparisons. Significance was determined for each variant protein *versus* wild-type SmTAL1: not significant (ns) P > 0·05; ** P ≤ 0.01; **** P ≤ 0.0001 Values are shown ± SEM; n = 3. It should be

noted that DSF measures complex, cooperative unfolding events and so K_d values estimated by this method are referred to as apparent values.

Table 2: **SmTAL1 ligand binding as revealed by differential scanning fluorimetry and chemical crosslinking.**

	Ligand	
	PZQ	**SmIQ3**
DSF		
Best fit	3PL ^{ns}	4PL ****
$K_{d, app}$ (µM) (± SEM)	143 ± 21	23.0 ± 1.6
Hill Slope (± SEM)	1 (by definition)	2.0 ± 0.2
R-square	0.94	0.98
Densitometry		
EC_{50} (µM) (± SEM)	Nd	28.2 ± 9.6
R-square	Nd	0.96

DSF data were fitted to either a 3PL or 4PL model, by non-linear regression. The model that represented the best fit to the data was chosen (as judged by the R-square value, and the extra-sum-of-squares, F-test). If 3PL and 4PL models were not significantly different (^{ns}), the simpler (3PL) model was chosen. SmIQ3 binding data deviated significantly from the simpler model (**** $P \leq 0.0001$; F-test; n = 3). The apparent dissociation constant ($K_{d, app}$), and Hill slope (h) were then derived from the plots. Densitometry data were fitted to equation 1 to determine the half maximal effect (EC_{50}). All fitting and analysis were performed in GraphPad Prism, v.6.0. The K_d values estimated here are larger than the EC_{50} for tonic contraction of the parasite's musculature (200 nM [82]). This may reflect the apparent (rather than absolute) nature of the K_d values or the existence of multiple targets for PZQ.

Table 3 **Screens of the open access Malaria box, plate A, as revealed by differential scanning fluorimetry.**

Well	MMV ID	CHEMBL ID	Structure	ΔT_m *vs* DMSO	Phenotype
A08	MMV019406	535730	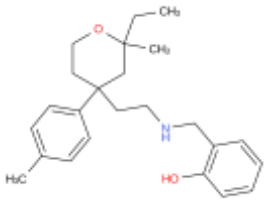	↑ 1.0 °C (*)	2 (24 hrs) 2 (48 hrs) 4 (72 hrs)
B10	MMV008416	601957	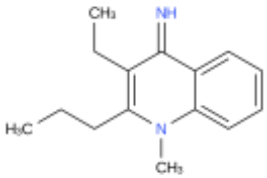	↓ 0.93 °C (*)	1 (24 hrs) 0 (48 hrs) 0 (72 hrs)
D03	MMV666596	1615697	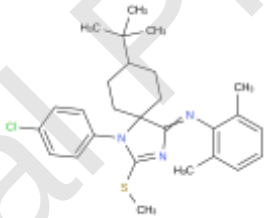	↑ 1.03 °C (*)	1 (24 hrs) 1 (48 hrs) 0 (72 hrs)
D11	MMV665831	535079	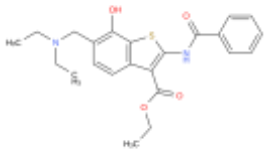	↑ 0.9 °C (*)	0 (24 hrs) 0 (48 hrs) 0 (72 hrs)

E03	MMV000642	578952	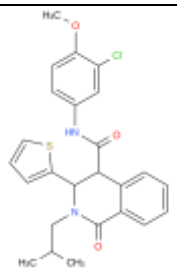	↑ 1.17 °C (***)	0 (24 hrs) 0 (48 hrs) 0 (72 hrs)
G06	MMV007686	601348	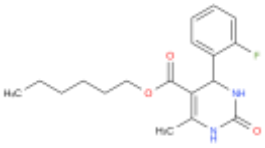	↑ 1.17 °C (**)	0 (24 hrs) 0 (48 hrs) 0 (72 hrs)

Eighty drug-like and probe-like compounds from the Malaria box plate A (at a final concentration of 100 µM), were screened for their ability to induce a thermal stability change in SmTAL1 (10 µM), when incubated in the presence of calcium chloride (1 mM). Six of these compounds were defined as "hits", based on a statistically significant increase (↑), or decrease (↓) in T_m *versus* the DMSO (1 % v/v) vehicle-only control group. Significance was determined using one-way ANOVA in GraphPad Prism 6.0 followed by Tukey's post hoc test for multiple comparisons: * P ≤ 0.05; ** P ≤ 0.01; ***P ⩽ 0·001 (± SD; n = 3). The identifiers, A3, B10, D3, D11, E3 and G6, denote the well numbers for each compound (based on the map for plate A; batch number: April 2013). Detailed information is available online at: https://www.mmv.org/research-development/open-source-research/open-access-malaria-box. All structures were accessed at ChEMBL EMBL-EBI (https://www.ebi.ac.uk/chembl/). Phenotype assays were conducted by the Caffrey group (University of California, San Francisco) measuring the effects of 2.5 µM compound on new transformed somules at24 h. Effects were scored using an arbitrary scale from 0 (no effect) to 4 (mostly dead). Data from this study was accessed online at: doi: 10.6019/CHEMBL2363022

Table 4: **SmIQ3 peptide binding data for Ca^{2+}-SmTAL in the presence of rising concentrations of PZQ, as revealed by differential scanning fluorimetry**

	Parameter		
	$K_{d,\ app}$ (µM) (± SEM)	**$\Delta T_{m,\ max}$ (°C) (±SEM)**	**R-square**
DMSO (1 %)	27.1 ± 2.9	2.5 ± 0.1	0.97
PZQ (20 µM)	14.9 ± 1.9 *	2.3 ± 0.1 ^{ns}	0.94
PZQ (40 µM)	11.9 ± 1.5 **	2.1 (± 0.1 ^{ns}	0.94
PZQ (80 µM)	14.4 ± 2.4 *	1.6 ± 0.1 **	0.91
PZQ (160 µM)	17.4 ± 3.5 ^{ns}	1.4 ± 0.1 ***	0.81
PZQ (300 µM)	7.9 ± 1.5 ***	1.2 ± 0.1 ****	0.87
PZQ (500 µM)	8.5 ± 2.1 **	0.9 ± 0.1) ****	0.84
Global fit parameters			
Hill slope (± SEM)	1.4 (± 0.1)		
R-square	0.93		

Data from Figure 9 were fitted to a hyperbolic binding equation, using nonlinear regression in GraphPad Prism v6.0. The Hill slope was constrained to a constant value of 1.4, and the apparent dissociation constant ($K_{d,\ app}$), and maximum change in thermal stability ($\Delta T_{m,\ max}$) (°C), were fitted. Statistical significance was determined for each PZQ treatment group *versus* the untreated (DMSO) treatment group, using one-way ANOVA followed by Tukey's post-hoc test for multiple comparisons: not significant (ns) P > 0·05; * P ≤ 0.05; ** P ≤ 0.01; *** P ≤ 0.001; **** P ≤ 0.0001 (n = 3).